1972

Experimental study and analog simulation of a jet interaction amplifier

Shiraz Yusuf Rehmani
Lehigh University

EXPERIMENTAL STUDY AND ANALOG SIMULATION OF A JET INTERACTION AMPLIFIER

Shiraz Yusuf Rehmani

ABSTRACT

An analytical and experimental study was conducted for predicting the steady state and dynamic response of a jet interaction fluid amplifier. The analysis is based on a physical model using a lumped parameter approach. The dynamics of the control and receiver lines together with various interacting fluid phenomenon occurring within the amplifier are examined. Flow resistances are determined experimentally and the resulting values used in the analytical model.

The dynamic model is presented in an analog format suitable for simulation on a digital computer.

Experimental studies were conducted on a large scale plexiglass model designed and developed in a previous study. This model amplifier operates at room temperature with air as the working fluid.

It is shown, by comparison of calculated and measured operating characteristics, that the performance of this type of amplifier can be predictbd to a reasonable degree of accuracy.

EXPERIMENTAL STUDY AND ANALOG SIMULATION OF A JET INTERACTION FLUID AMPLIFIER

by

Shiraz Yusuf Rehmani

A Thesis
Presented to the Graduate Committee
of Lehigh University
in Candidacy for the Degree of
Master of Science
in
The Department of Mechanical Engineering and Mechanics

Lehigh University
1972

This thesis is accepted and approved in partial fulfillment of the requirements for the degree of Master of Science.

June 29, 1972
(date)

James P. Ries
Professor in Charge

Ferdinand F. Bear
Chairman of Department

ACKNOWLEDGEMENT

Throughout this study, the author received most valuable guidance from his teacher and thesis adviser, Dr. James P. Ries, to whom the author wishes to express his gratitude.

The work was supported by the Office of Naval Research under Contract No. N00014-69-A-0417.

TABLE OF CONTENTS

LIST OF FIGURES

ABSTRACT

An analytical and experimental study was conducted for predicting the steady state and dynamic response of a jet interaction fluid amplifier. The analysis is based on a physical model using a lumped parameter approach. The dynamics of the control and receiver lines together with various interacting fluid phenomenon occurring within the amplifier are examined. Flow resistances are determined experimentally and the resulting values used in the analytical model.

The dynamic model is presented in an analog format suitable for simulation on a digital computer.

Experimental studies were conducted on a large scale plexiglass model designed and developed in a previous study. This model amplifier operates at room temperature with air as the working fluid.

It is shown, by comparison of calculated and measured operating characteristics, that the performance of this type of amplifier can be predicted to a reasonable degree of accuracy.

NOMENCLATURE

A	cross-sectional area of flow channels
a	integration limit
B	setback
b	integration limit
C	fluid compliance
F	empirical factor
H	amplifier height
I	fluid inertance
J	momentum of jet
K	ratio of specific heats
L	amplifier jet flow length
ℓ	length of flow channels
M	dynamic pressure intercepted by receiver
$\dot{m}$	mass flow rate
P	pressure
R	fluid resistance
Rg	gas constant for air
Re	Reynolds number
T	temperature
t	time
U	center line velocity
u	local velocity
V	magnitude of velocity for flat velocity profile
v	volume

W	width
x	distance combined jet travels measured from apparent point of emanation along axis of deflection
y	distance measured orthogonal to axis of deflection
γ	splitter angle
θ	deflection angle
σ	Goertler spread parameter
ρ	density

Subscripts

a	ambient
c	control
e	exit conditions from receiver
n	index in fluid resistance law
o	conditions at formation of contained jet
R	conditions at receiver
s	supply
cl	control line
c1	control line
c2	control line - channel interface
c3	control channel
c4	control port
R1	receiver tank-line interface
R2	receiver line

1. INTRODUCTION

The jet interaction fluid amplifier was conceived by B. M. Horton of the Harry Diamond Laboratories. It makes use of the principle of momentum exchange between orthogonal fluid jets to obtain proportional fluid amplification. Figure (1) shows the jet interaction amplifier and its typical characteristics.

In the absence of control inputs, the power jet divides against the center splitter and provides equal flows in the receiver channels. With a differential flow applied across the control ports, bending of the power jet takes place. A small amount of power jet deflection provides significant changes in the differential flow from the right and left receiver channels. Power gains of 10 with pressure gains of 5 to 7 are currently obtained per stage in cascades of jet interaction amplifiers.

Even though feasible applications of the amplifier are now recognized in many different fields, the true potential of the device can only be realized as its dynamic behavior is understood in more depth and in more detail. To this end, a number of studies have been conducted and various dynamic models have been proposed, both for the vented amplifier and for the amplifier with internal feedback. These models have fallen into either of the two

categories: (1) the functional model, which uses the black-box approach and (2) the physical model which considers the details of the internal processes and relates them to terminal properties.

This study is an extension to previous work [4] employing a physical model with system equations developed in a form amenable to solution by an analog simulation program run on a digital computer.

The two-dimensional, incompressible analysis is performed by considering the amplifier to consist of three parts: control region, mainstream and the combined receiver load region. The main assumptions are that the interaction region remains approximately at atmospheric pressure and the amplifier can be described by lumped parameter methods for the purpose of dynamic studies.

Attention is focussed on developing a model for the receiver-jet interface region using a control volume approach. The region of interaction of the supply and control jets is also considered in some detail. Again, using the control volume approach, jet deflection angles are predicted.

To provide a check on the accuracy of the analysis, steady state and dynamic tests were conducted on a large-scale experimental amplifier developed in the previous

study [4]. Dynamic tests consisted of subjecting the amplifier to a step input signal, and monitoring the resulting response.

2. ANALYTICAL STUDY

2.1 Introduction

This study attempts to model the various fluid phenomenon occurring within the different regions of the jet interaction amplifier. This analysis will, hopefully, lead to a complete analog model for the amplifier which can predict its dynamic response to various inputs.

Owing to the complexity of the system equations associated with these fluid phenomenon, only a very simplified, two-dimensional, incompressible analysis is attempted. The mathematical relations involving the physical variables are stated in a form amenable to solution by an analog simulation program run on a digital computer.

The regions of interest which are analyzed are:

(a) Control port and the associated tubing connecting it to the pressure plenum.

(b) Jet interaction region.

(c) The region of subsequent development of combined jet.

(d) Receiver port and its associated loading.

2.2 Control Port Dynamics

Two alternatives are available in modelling the dynamics of the control port and its associated line. Both methods

are computer oriented [3] and have been found to successfully model the dynamics. These are:

(a) The lumped parameter model.

(b) The distributed parameter model.

The lumped parameter model has been preferred for this study since it is relatively simple and can be easily incorporated into an analog simulation program. It employs the analogy between electric current flow and fluid flow, thus mass flow rate corresponds to current, pressure to voltage and fluid resistance to electric resistance. Also for a time varying flow, capacitive and inductive impedances are introduced which correspond to resistances due to mass storage and momentum storage respectively. The lumped parameter model does not consider the interaction of these controlling resistances, but merely lumps them together in their spatial dimensions.

The control line is separated into two sections: (1) the line from control plenum to amplifier control port, and (2) the control channel within the amplifier itself. Since the amplifier is vented, the pressure in the jet interaction region is assumed to be at ambient pressure P_a. A time varying input pressure signal, P_c, is imposed on the control line while exit pressure is assumed to be held constant; this results in a time varying control flow due to control line dynamics.

The control line variables used in the model are shown in Figure (2). The pressure drops in the line caused by frictional resistances are given by the general formula:

$$\Delta P = R\dot{m}^{n}$$

The pressure drop due to inertance is determined by the following equation used by Heck [4]

$$\Delta P = I \frac{d\dot{m}}{dt}$$

where $I = \ell/A$

The impedances of the line to a changing pressure may be expressed as [4]

$$\Delta\dot{m} = C \frac{dP}{dt}$$

where $\Delta\dot{m}$ is the difference in the input and output flow rates of the section of the line concerned

and $C = v/RgT$ for isothermal flow

or $C = v/KRgT$ for adiabatic flow

Hence a complete set of equations, representing the various pressure drops can now be written as follows:

$$P_c - P_{c1} = I_1 \frac{d\dot{m}_1}{dt} \qquad 2.1$$

$$P_{c1} - P_{c2} = R_{c1} (\dot{m}_1)^{n1} \qquad 2.2$$

$$\dot{m}_1 - \dot{m}_3 = C \frac{dP_2}{dt} \qquad 2.3$$

$$P_{c2} - P_{c3} = I_3 \frac{d\dot{m}_3}{dt} \qquad 2.4$$

$$P_{c3} - P_{c4} = R_{c3} (\dot{m}_3)^{n3} \qquad 2.5$$

$$P_{c4} - P_a = R_{c4} (\dot{m}_3)^{n4} \qquad 2.6$$

The values of the resistances, R, and exponents n are obtained experimentally while the values of C and L are obtained from the indicated relations.

For the steady state case in which a constant control pressure P_c is imposed on the control line, equations 2.1 to 2.6 reduce to:

$$P_c = P_{c1} \qquad 2.1a$$

$$P_{c1} - P_{c2} = R_{c1} (\dot{m}_1)^{n1} \qquad 2.2a$$

$$\dot{m}_1 = \dot{m}_3 \qquad 2.3a$$

$$P_{c2} = P_{c3} \qquad 2.4a$$

$$P_{c3} - P_{c4} = R_{c3} (\dot{m}_3)^{n3} \qquad 2.5a$$

$$P_{c4} - P_a = R_{c4} (\dot{m}_3)^{n4} \qquad 2.6a$$

Or denoting the constant control flow as $\dot{m}_c$

$$P_c - P_{c3} = R_{c1} (\dot{m}_c)^{n1} \qquad 2.7a$$

$$P_{c3} - P_{c4} = R_{c3} (\dot{m}_c)^{n3} \qquad 2.7b$$

$$P_{c4} - P_a = R_{c4}(\dot{m}_c)^{n4} \qquad 2.7c$$

The jet emerging from the control port into the interaction region is assumed to have a flat velocity profile so that the control mass flow rate is given by

$$\dot{m}_3 = \dot{m}_c = \rho H W_c V_c \qquad 2.7d$$

2.3 Jet Interaction Region

Although the experimental amplifier provides for two control ports opposite each other and perpendicular to the supply jet, for analysis purposes, only one control jet is introduced. The interaction region, therefore, consists of the main supply jet with the control jet impinging at right angles to it. Is is assumed that the static pressure throughout the interaction region is constant and equal to the ambient pressure P_a. The Bernoulli equation is used to relate the supply pressure and supply velocity:

$$P_s = \frac{1}{2}\rho V_s^2 \qquad 2.8$$

Following the work of Moses [9], the control volume being considered is shown in Figure (3). Equating the pressure forces to the momentum in the vertical direction, one obtains,

$$J_s \tan\theta - J_c = W_c H P_{c4}'$$

where

$$J_s = \rho V_s^2 W_s H$$

$$J_c = \rho V_c^2 W_c H$$

and

$$P_{c4'} = P_{c4} - \frac{1}{2} \rho V_c^2$$

then

$$\tan\theta = \frac{1}{2}\left(\frac{V_c}{V_s}\right)^2 \frac{W_c}{W_s} + \frac{W_c}{W_s} \frac{P_{c4}}{\rho V_s^2}$$

but

$$P_s = \frac{1}{2} \rho V_s^2$$

hence

$$\tan\theta = \frac{1}{2} \frac{W_c}{W_s} \left[\left(\frac{V_c}{V_s}\right)^2 + \frac{P_{c4}}{P_s}\right] \qquad 2.9$$

2.4 Region of Subsequent Development of Combined Jet

The analysis for the development of a single submerged jet is extensively reported in literature [2, 15]. The discussion for the velocity profiles of a turbulent jet concerns the region in which the flow is fully developed. The various regions of a turbulent jet are [6] the potential core, the mixing region, the transition region and the fully developed region. The potential core formed when the jet is discharged from the nozzle is gradually penetrated by the mixing layers. Also, the fluid entrained by the jet leads to a gradual spreading of the jet.

The assumptions made regarding shear stress for the derivation of velocity profiles of the turbulent jet are numerous and of a semi-empirical nature. From Prandlt's hypothesis, which makes use of Boussinesq's eddy kinematic viscosity, Schlichting [14] arrives at the Goertler's profile for a turbulent jet:

$$u = U \operatorname{sech}^2\left(\frac{\sigma y}{x}\right)$$

Although this submerged jet analysis does not apply directly to perpendicularly interacting jets, the velocity profiles established further downstream of the interaction region are similar. Also, the three-dimensional effects imposed by the top and bottom plates are not accounted for in this formulation. It has been experimentally established that after the interaction region, the two jets merge, even though the velocity profile is initially bilobular. However, further downstream of the interaction region, velocity profiles resembling the Gaussian profiles are obtained. Furthermore, the merging of the two lobes of the initial velocity profile into a single lobe due to large turbulent shearing stresses, accounts for the vena contracta effect observed by Sarpkaya [13]. It has been empirically established that the profile becomes Gaussian in a distance of $4W_c$ and that the vena contracta effect extends, at the most, to $2W_c$.

The control volume approach to determining the jet deflection was adopted because the actual phenomenon occurring within the interaction region is not well understood. It is further postulated that the Goertler profile is established $2W_c$ downstream of the supply port with the supply jet pivoting at the intersection of the center lines of the supply and control ports. The latter assumption is somewhat doubtful since Abramovich's [1] study shows the pivot point of the jet to be dependent on the ratio of W_c/W_s and for a ratio of 2 it is slightly away from the center. However, the difference is small and no modification is made.

The jet at a distance of $2W_c$ from the supply port has the mass flow equal to the sum of the supply and control jet flows. Neglecting energy lost due to shear action at top and bottom plates, the momentum is also the sum of the momenta of the supply and control jets at this point.

Using the control volume shown in Figure (4), a mass balance gives

$$W_s V_s + W_c V_c = 2U_o \int_o^\infty \operatorname{sech}^2 \frac{\sigma y}{x}\, dy \Big|_{x=x_o}$$

$$= 2U_o \frac{x_o}{\sigma} \qquad 2.10$$

where x_o is the distance from the apparent point of emanation

of the combined jet to the point where the Goertler profile is assumed to be established and measured along the axis of deflection of the combined jet.

From Figure (4), a momentum balance gives:

$$W_s V_s^2 + W_c V_c^2 = 2U_o^2 \int_o^\infty \operatorname{sech}^4 \left(\frac{\sigma y}{x}\right) dy \Big|_{x=x_o}$$

$$= \frac{4}{3} U_o^2 \frac{x_o}{\sigma} \qquad 2.11$$

Solving equations 2.10 and 2.11 simultaneously yields

$$\frac{U_o}{V_s} = \frac{3}{2} \frac{1 + W_c/W_s (V_c/V_s)^2}{1 + W_c/W_s \; V_c/V_s} \qquad 2.12$$

and

$$\frac{x_o}{\sigma} = \frac{W_s}{3} \frac{(1 + W_c/W_s \; V_c/V_s)^2}{1 + W_c/W_s (V_c/V_s)^2} \qquad 2.13$$

In these relations, σ is the spread parameter for the Goertler velocity profile and a value of $\sigma = 7.67$ suggested by Reichardt is used.

As the combined jet proceeds downstream, it behaves as a fully developed submerged jet with its center line velocity U_o decaying parabolically. Hence from the geometry of the amplifier in Figure (5) and the deflection angle, one obtains for the center line velocity at the receiver

$$U_R = U_o \sqrt{\frac{x_o}{x_R}} \qquad 2.14$$

$$x_R = x_o + (L - 2W_c)/\cos\theta \qquad 2.15$$

Variable x_R is the distance the jet has travelled along its axis of deflection from its apparent point of emanation, before encountering the receiver.

2.5 Interaction of Combined Jet With Receiver

Manion [7] and Rupert [12] have given a method to account for the effect of receiver loading on the receiver flow $\dot{m}_R$.

For a given velocity distribution, Olson and Camarata [10] point out, [Figure (6)], that the flow entering the receiver port may be greater than or less than the portion of the profile intercepted by the receiver. In addition, experimental data is given by Kallevig [5] which shows that the pressure acting on the receiver is that due to the portion of the dynamic pressure intercepted by the receiver even when the receiver is completely blocked.

On this basis experimental studies were conducted and it was found that, although for the case when flow is allowed through the receiver reasonable prediction of receiver pressure could be made by taking the intercepted dynamic pressure profile, virtually no agreement was obtained when the receiver was blocked. This suggested a needed modification

in the model. Writing momentum conservation equation for the control volume shown in Figure (7) and assuming that flow out of the control volume into the receiver is one-dimensional,

$$\rho H \int_{-a}^{b} [u \cos(\gamma-\theta)]^2 dy \Big|_{x=x_R} + P_a W_R H = P_R W_R H + \rho V_R^2 H W_R$$

$$\rho U_R^2 \cos^2(\gamma-\theta) \int_{-a}^{b} \operatorname{sech}^4 \frac{\sigma y}{x_R} dy = (P_R - P_a) W_R + \rho V_R^2 W_R$$

$$M = (P_R - P_a) W_R + \rho V_R^2 W_R$$

where M is the dynamic pressure intercepted by the receiver.

$$M = \rho U_R^2 \cos^2(\gamma-\theta) \{ \frac{x_R}{3\sigma} [\tanh(\frac{\sigma b}{x_R}) (\operatorname{sech}^2 \frac{\sigma b}{x_R} + 2)$$

$$+ \tanh \frac{\sigma a}{x_R} (-\operatorname{sech}^2 \frac{\sigma a}{x_R} + 2)] \}$$

The integration limits a and b are determined from the geometry of the amplifier as shown in Figure (5)

$$a = (L - \frac{W_c}{2}) \frac{\sin\theta}{\cos(\theta-\gamma)} \qquad 2.16$$

$$b = W_R - a \qquad 2.17$$

It is now postulated that owing to the effect of receiver loading only a fraction (F) of the dynamic pressure profile intercepted by the receiver port represents the actual momentum influx into the control volume, so that the

momentum equation now reads

$$M(F) = (P_R - P_a)\, W_R + \rho W_R V_R^2 \qquad 2.18$$

where the factor (F) is determined experimentally.

2.6 Modelling of the Receiver Port and Associated Line

The steady state and dynamic modelling of the receiver are considered separately so that a complete set of performance characteristics for the steady state case can be obtained.

For the steady state case, the pressure drops in the receiver port and line due to frictional resistances to flow are determined experimentally as in the case of the control port. A linear resistance is used in the line with its far end exposed to the ambient pressure P_a, so that the corresponding pressure drop becomes

$$P_R - P_a = R_R \dot{m}_R \qquad 2.19$$

Substituting into equation 2.18 and noting that $V_R = \dot{m}_R / \rho H W_R$, one obtains

$$\frac{M(F)}{W_R} = R_R \dot{m}_R + \dot{m}_R^2 / \rho H^2 W_R^2 \qquad 2.20$$

For the case in which the receiver is blocked, there is no flow out of the control volume and hence the second term on the right hand side of eqn. 2.18 vanishes, so that

$$\frac{M(F)}{W_R} = (P_R - P_a) \qquad 2.21$$

Dynamic modelling of the receiver takes into account the impedances due to capacitive and inductive loading. The equations for the corresponding pressure drops are similar to those for the control port. Using the variables identified in Figure (8), one obtains

$$\dot{m}_R - \dot{m}_e = C_R \frac{dP_{R1}}{dt} \qquad 2.22$$

$$P_{R1} - P_{R2} = I_R \frac{d\dot{m}_e}{dt} \qquad 2.23$$

$$P_{R2} - P_a = R_R \dot{m}_e \qquad 2.24$$

where I_R and C_R are obtained from the loading geometry.

The F factor for each of the two steady state cases (i. e. finite resistance and blocked receiver) is determined experimentally. The value obtained for the finite resistance case is also used for predicting the dynamic response of the amplifier.

It should be pointed out that the actual flow into the receiver, $\dot{m}_R$, does not correspond to flow supplied by the interception of the velocity profile by the receiver but is determined by the load characteristics of the receiver and line. The remaining portion of the flow is spilled on both sides of the receiver.

2.7 Steady State Model for the Amplifier

In the steady state case, a constant pressure P_c is applied to the control port. The three linear, algebraic equations 2.7a, 2.7b and 2.7c predict the pressure drops in the channel with equation 2.7d giving a constant control velocity V_c and equation 2.9, a constant deflection angle θ. Equations 2.12, 2.13, 2.14, 2.15 and 2.18 then predict the steady state response of the amplifier to any control pressure P_c and supply pressure P_s.

A computer program was written which calculates receiver pressure and mass flow rate for any supply and control pressure. The results were compared with experimental values for three different values of supply pressure P_s and various control pressures, P_c, to determine the F factor both for the finite resistance and the blocked receiver cases.

2.8 LEANS Model for the Dynamic Response of the Amplifier

The dynamic model for the amplifier consists of seventeen coupled equations and eighteen physical variables, most of which can be experimentally determined. For a known input signal P_c, the response of the amplifier may be determined. The analytical model is represented in standard analog form in Figure (9), with numerical indices indicating

corresponding equation numbers.

The model has been adapted as in the previous study [4] to a computer code LEANS [8], which simulates an analog computer on the CDC 6400 digital machine. It employs the block diagram technique commonly considered the first step of any analog simulation. There is a full array of integrators, constants, summers, nonlinear blocks, etc. which are used as interconnecting elements. Programming directly from the block diagram is possible since time and magnitude scaling are unnecessary for a machine using floating point arithmetic.

Changes in various flow parameters are easily incorporated into the program as physical models of the different fluid phenomenon occurring in the various sections of the amplifier are altered.

3. EXPERIMENTAL STUDY

3.1 Amplifier Design and Test Rig

Steady state and dynamic tests were conducted on a large-scale plexiglass model amplifier which was designed in the previous study [4], the geometry of the amplifier conforming to optimum dimensions suggested by Powell and Bidgood [11]. The average dimensions about which the geometry was varied are:

Setback B	=	$2W_s$
Channel height H	=	$2W_s$
Control port width W_c	=	$2W_s$
Receiver port width W_R	=	$2W_s$
Amplifier length L	=	$10W_s$
Splitter angle γ	=	12°

The optimum geometry of the amplifier was arrived at [4] through a similarity analysis, with the Reynolds number and Strouhal number as scaling parameters. Further steady state testing was done to check the performance of the amplifier. It was found that parallel control channel entrance gave identical steady state output results as a perpendicular entrance but the latter gave a higher noise level in the output. A control width of $2W_s$ and a setback of B = 0.50 inches was found to give the best overall amplifier performance. The final geometry of the optimized amplifier is shown in Figure (10).

3.2 Instrumentation

The amplifier model is integrated into a bench configuration, which allows variation of supply flow up to a Reynolds number of 10^5. Regulators are used to set the supply and control pressures while rotameters measure the resulting flows. A number of static pressure taps are located at various points in the amplifier for static pressure measurements.

A plenum followed by an electrically operated pneumatic switch is introduced in the control line. The input pressure signal, which is a step up in pressure from the ambient pressure condition, is monitored by a Statham strain gauge pressure transducer mounted flush in the control line. A similar transducer mounted in the receiver tank, (which is connected to the receiver channel and presents a capacitive loading), picks up the output response to the input step signal. The total nonlinearity and hysteresis of the transducing cell and pressure diaphragm is a maximum of ±0.25% full-scale. The transducer signals are amplified by Statham bridge amplifiers. The output of the amplifier can be used to study the signals through a storage unit type oscilloscope or can be recorded on a Brush strip chart recorder. A schematic diagram of the complete experimental set-up is shown in Figure (11).

The pneumatic switch valve used to produce a step up signal is of the "normally closed" type so that flow is allowed into the control channel only when the valve is switched. The actual signal from this valve, as monitored by the transducer, is not exactly a step. There is, in fact, an overshoot before the pressure comes to the desired final value. However, the response time is small enough so that the signal can be approximated by a simple step up.

3.3 Experimental Determination of Resistances

A number of fluid resistances are encountered in the analytical modelling of the amplifier. They correspond to the different sections of the amplifier: (1) the control line, (2) the control channel, (3) setback of control port and (4) the receiver line.

The values of these resistances are obtained experimentally by steady state tests. These consist of measuring the static pressure at the various points indicated in Figure (11) in the control and receiver lines and monitoring the corresponding constant control and receiver flows. The testing was done for a number of supply and control pressures. Plots on a log-log scale of the pressure drops against corresponding flow yields the values for both the resistance R and exponent n for all the four sections considered. These plots are shown in Figures (12 to 19).

3.4 Steady State Performance of Amplifier

Steady state tests were conducted for both the finite resistance and blocked receiver case with three values of supply pressure namely P_s = 4, 5 and 6 inches of water. For the finite resistance case, with each of these supply pressures, the receiver pressure P_R and mass flow rate $\dot{m}_R$ were measured for a variety of control pressures P_c. The procedure was repeated for the blocked receiver with the only measured output variable being the receiver pressure. The results were plotted and compared with those predicted by the steady state analytical model for different values of the F factor. The steady state characteristics of the amplifier, represented as plots of P_R versus P_c and $\dot{m}_R$ versus $\dot{m}_c$, are shown in Figures (16 to 24) together with the analytically predicted curves for the selected values of the F factor.

3.5 Dynamic Response of the Amplifier to a Step Input

The dynamic response of the amplifier was studied by monitoring the output pressure signal with a strip chart recorder. Due to edge-tone effect which is characteristic of a jet interacting with a splitter, large pressure fluctuations, extremely periodic and approximately sinusoidal were observed. This had considerable effect on the dynamic response of the amplifier. For the case of the undeflected

jet (P_c = 0), the magnitude of these fluctuations was greatest. For the case in which the jet was deflected to a position, corresponding to a maximum value of receiver pressure P_R, the fluctuations were of negligible magnitude.

It was found that the response of the amplifier to a step input depends on the switching point with respect to the edge-tone cycle. A faster response was observed when the switching occurred at such a point that the jet was already moving in the right direction. The slowest response was observed when switching occurred with the jet travelling in the opposite direction. Representative responses of the amplifier are plotted in Figures (26 and 27) for a supply pressure of P_s = 6 inches of water for two different points of switching.

4. ANALYTICAL AND EXPERIMENTAL RESULTS

4.1 Determination of the F Factor

The F factor which is indicative of the actual momentum influx into the receiver control volume was found to be a function of the receiver loading as expected. The F factor was determined from the steady state operation of the amplifier with two distinct cases being considered; (1) Finite, linear, receiver resistance and (2) Blocked receiver. For both these cases tests were run at three different values of supply pressure. The computer program for the steady state model of the amplifier was run for the same values of supply pressure, with F factor values varying from 1.0 to 0.1.

For the particular value of resistance used, a very good correlation between the experimentally obtained characteristics and the analytically predicted ones was obtained for all three values of supply pressure. These curves are shown in Figures (16 to 21). Also for the blocked receiver case a value of F = 0.145 gave good correlation between theory and experiment as shown in Figures (22 to 24).

Experiments were also run for higher values of supply pressure but analytical results failed to agree with

experiments. It was determined that the cause of this discrepancy was the receiver resistance becoming nonlinear for values of flow exceeding that corresponding to a supply pressure of six inches of water.

It was also experimentally observed that when the control pressure exceeded a certain limit, the receiver pressure changed very slightly for further increases in the control pressure. This is attributed to the fact that, beyond these values of control pressure, the jet attaches itself to the receiver wall opposite the splitter. It remains there until the control pressure is increased sufficiently so as to deflect it beyond the receiver wall. This jet attachment phenomenon was marked by the change in tone of the sound emitted by the experimental amplifier. This effect is clearly shown in the experimental characteristics by the flattening of the receiver pressure curves beyond certain values of the control pressure.

4.2 Deflection Angle θ

Means were not provided in the experimental set-up to make measurements of the jet deflection angle θ and provide a check on the predicted value of θ. However, the control pressure which gives the maximum receiver pressure should represent a jet deflection angle where the jet center line falls in the middle of the receiver channel. This is

approximately found to be the case for all the three values of supply pressure considered. For example for a value of P_s = 5 inches of water, the predicted value of the deflection angle is 6.0° compared to an experimental value of 5.8°.

4.3 Dynamic Response of Amplifier to a Step Input

The experimentally obtained dynamic response curves for two different switching points are shown in Figures (26 and 27). These were obtained for a value of supply pressure P_s = 6 inches of water and a control pressure step up from P_c = 0 to 1.5 inches of water. With the value of P_c = 1.5 inches of water, the jet is deflected such that its center line lies in the middle of the receiver channel.

The initial, analytical modelling of the amplifier did not consider the edge-tone effect of the jet oscillations. The dynamic response predicted by this analog model is shown in Figure (25). Comparing the experimental dynamic response with the analytical response is very difficult without the effect of the edge-tone modelled in the analog simulation. Hence, an attempt was made to model the edge-tone effect by imposing on the supply jet a sinusoidally varying deflection. The magnitude and frequency was sufficient to cause receiver pressure fluctuations resembling those obtained experimentally without any control flow. The dynamic response was then obtained by applying the control pressure step signal at various points with respect to the edge-tone cycle.

It was found in both the experimental and analytical dynamic response curves that the receiver pressure fluctuations due to edge-tone effect are of considerably smaller magnitude for the fully deflected jet, than that for the case of the undeflected jet. This provides an approximate check on the jet velocity distribution at the receiver interface, especially on the spread parameter σ. It also checks, to some extent, the order of magnitude of the parameters C and I used in the dynamic modelling of the receiver.

There is however, some disagreement between the dynamic response curves from the simulation and those obtained experimentally. This may be due to several factors. First, a lumped parameter approach was used to model the receiver and control lines. However, since the physical dimensions of the system are small with respect to the wave lengths of all flow variables, this cannot be considered as a major cause of the observed discrepancy.

The use of the steady state F factor for the dynamic case could be a more serious effect. Since in the dynamic case, the compliance and inertance of the receiver line impose further impedances to flow, the value of the F factor used should be the one corresponding to this new value of dynamic resistance rather than the steady state value. Other factors not considered in the model are due to the three-dimensional effects introduced by the cover plates.

However, considering the complexity of the entire amplifier and the undefined fluid flow patterns, the comparison between predicted and experimental response is quite acceptable.

5. SUMMARY

The purpose of this study was to present a model for the jet interaction type fluid amplifier so that its steady state and dynamic response characteristics could be obtained. Both were then compared with experimentally obtained responses.

Fluid resistances were all determined experimentally and the values were then used in the analytical model. Wherever possible, checks were provided on the other flow constants, which were determined from theoretical considerations.

The deflection angles predicted for various values of P_C and P_S were found to be comparable with the experimentally observed ones.

The empirical F factor representing the momentum influx into the receiver control volume was obtained experimentally for the two steady state cases considered. In both cases the agreement between the model and the experimental values for amplifier performance was good. The dynamic response predicted by the analog similation, using the steady state F factor, does not compare, as well as desired, with the experimentally obtained response. However, considering the complexity of the entire amplifier and the undefined fluid flow patterns, the comparison between predicted and experimental response is acceptable.

The introduction of the F factor could provide a starting point for further experimental investigation of the receiver characteristics. This would involve complete experimental determination of the F factor for various cases of static and dynamic loading of the receiver and a possible development of an analytical model for its prediction under various receiver loading conditions.

The simulation program is presented in such a form that changes in various flow parameters and load conditions can be easily incorporated into the model.

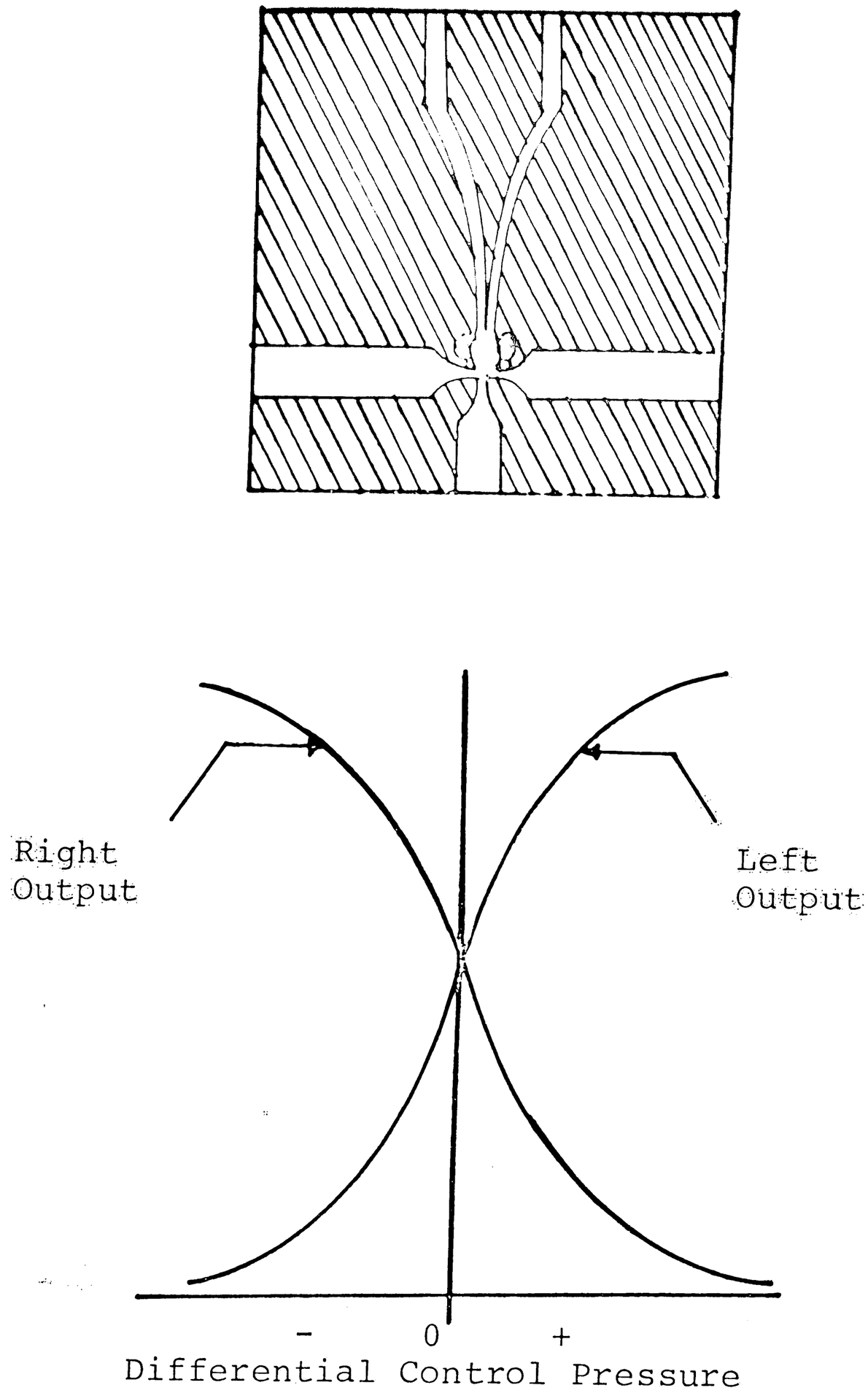

Figure 1. Pressure Characteristics of Typical Jet Interaction Amplifier.

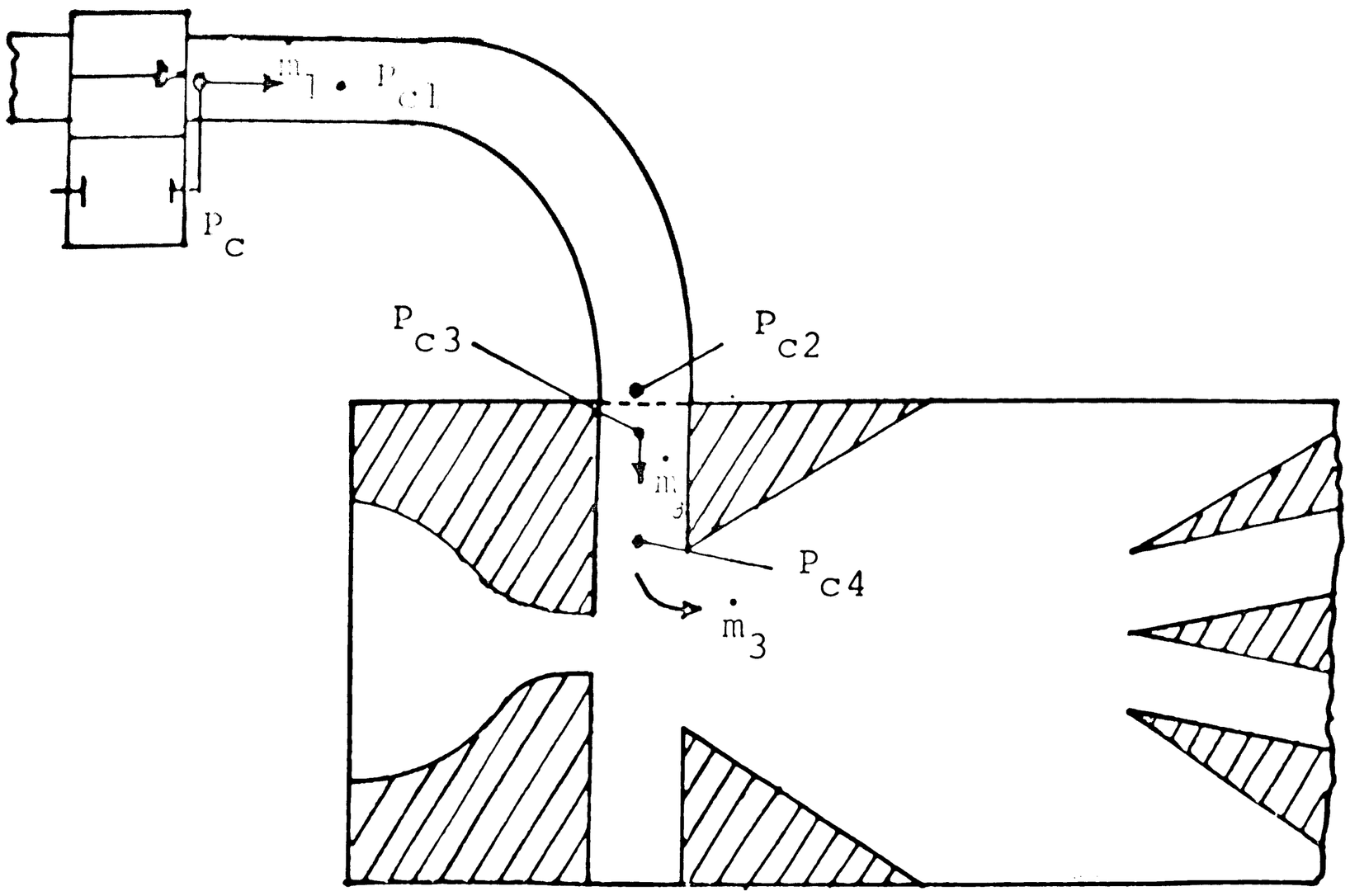

Figure 2. Control Line Model.

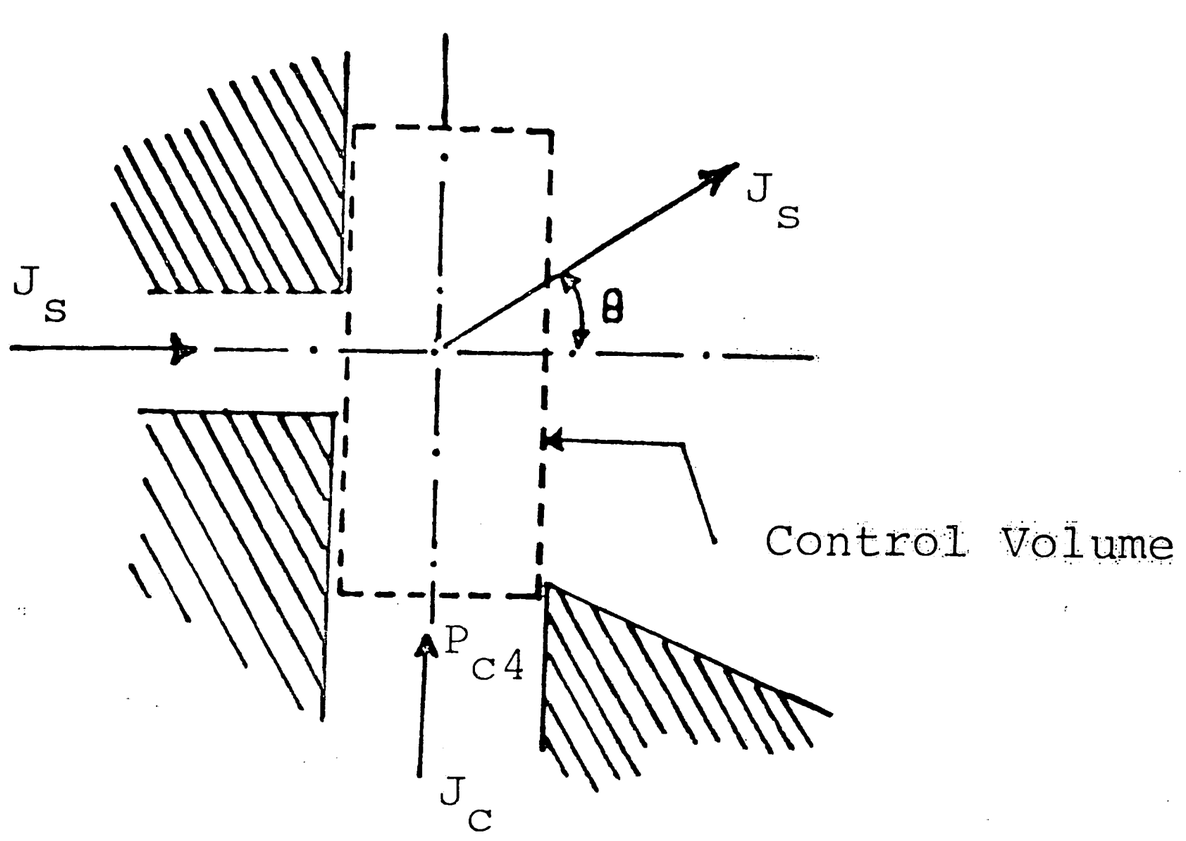

Figure 3. Control Volume for Jet Deflection.

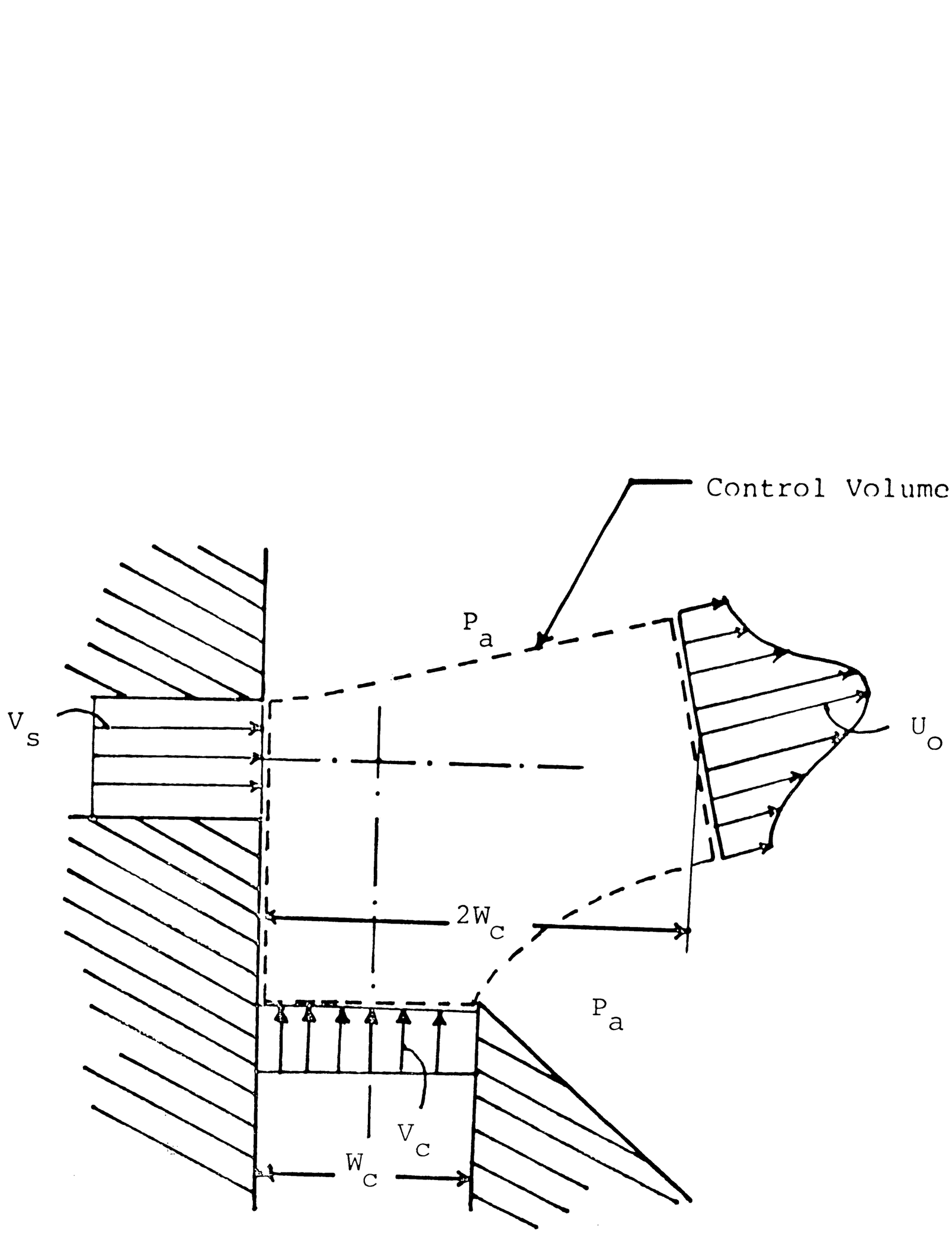

Figure 4. Control Volume for Jet Mixing.

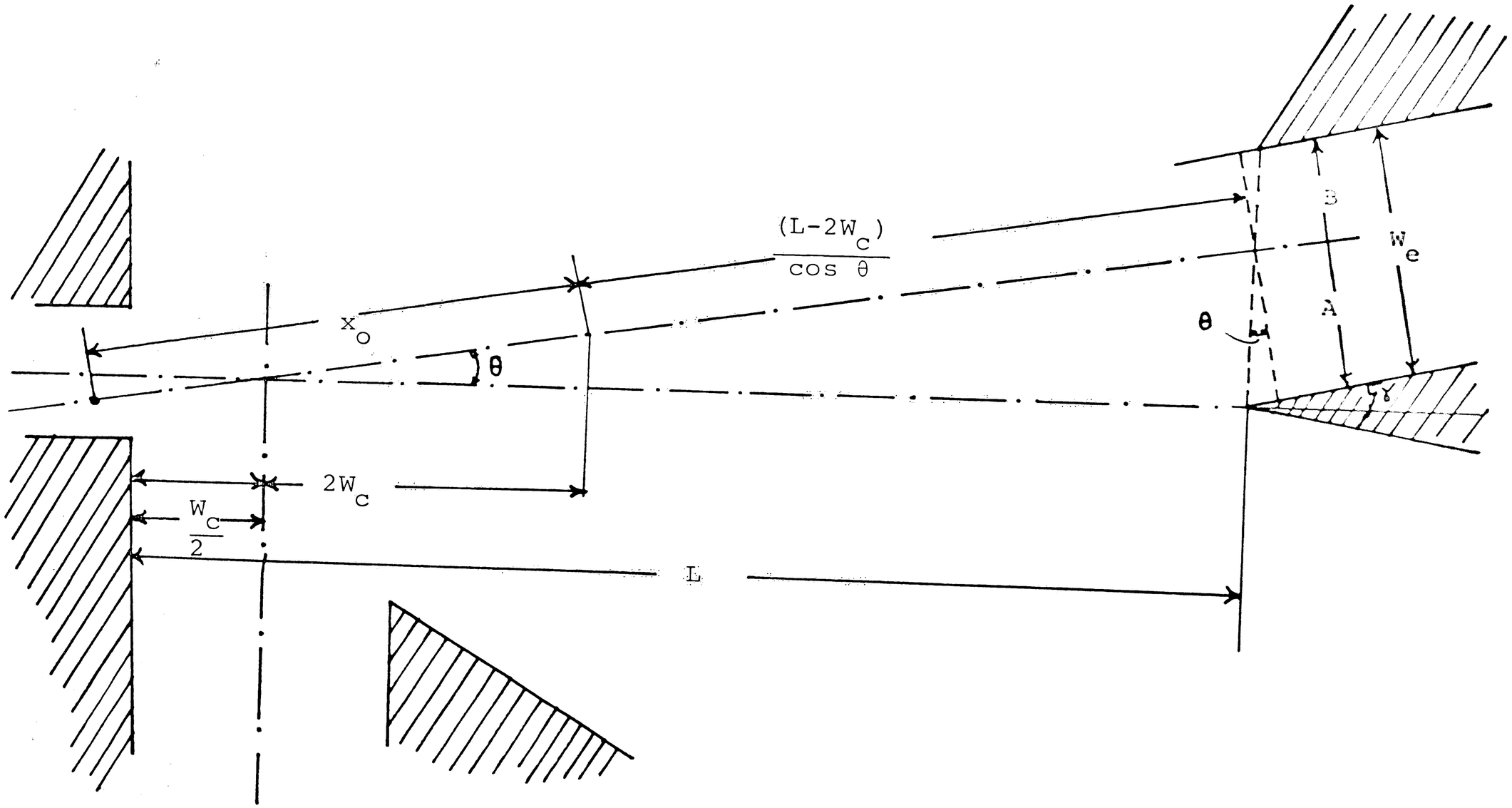

Figure 5. Receiver Geometry.

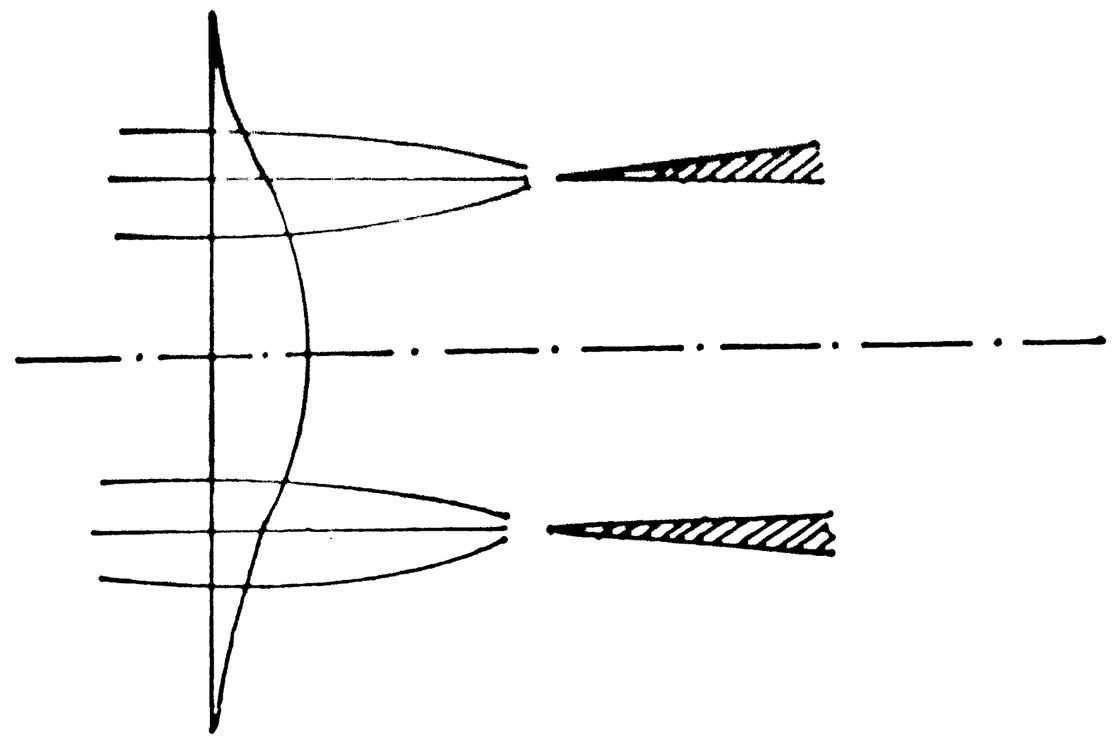

Finite Resistance Load

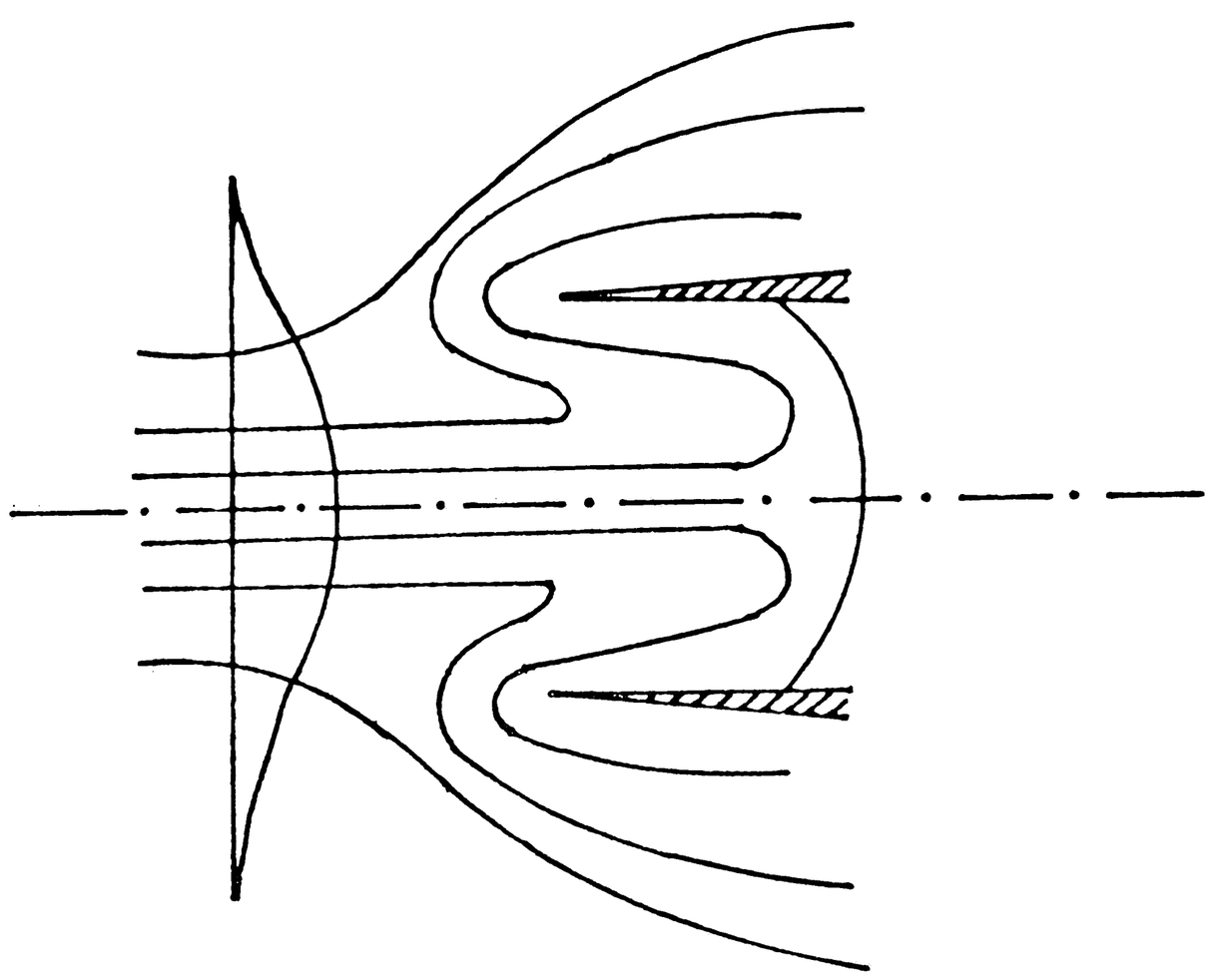

Blocked Receiver

Figure 6. Flow into a Receiver [10].

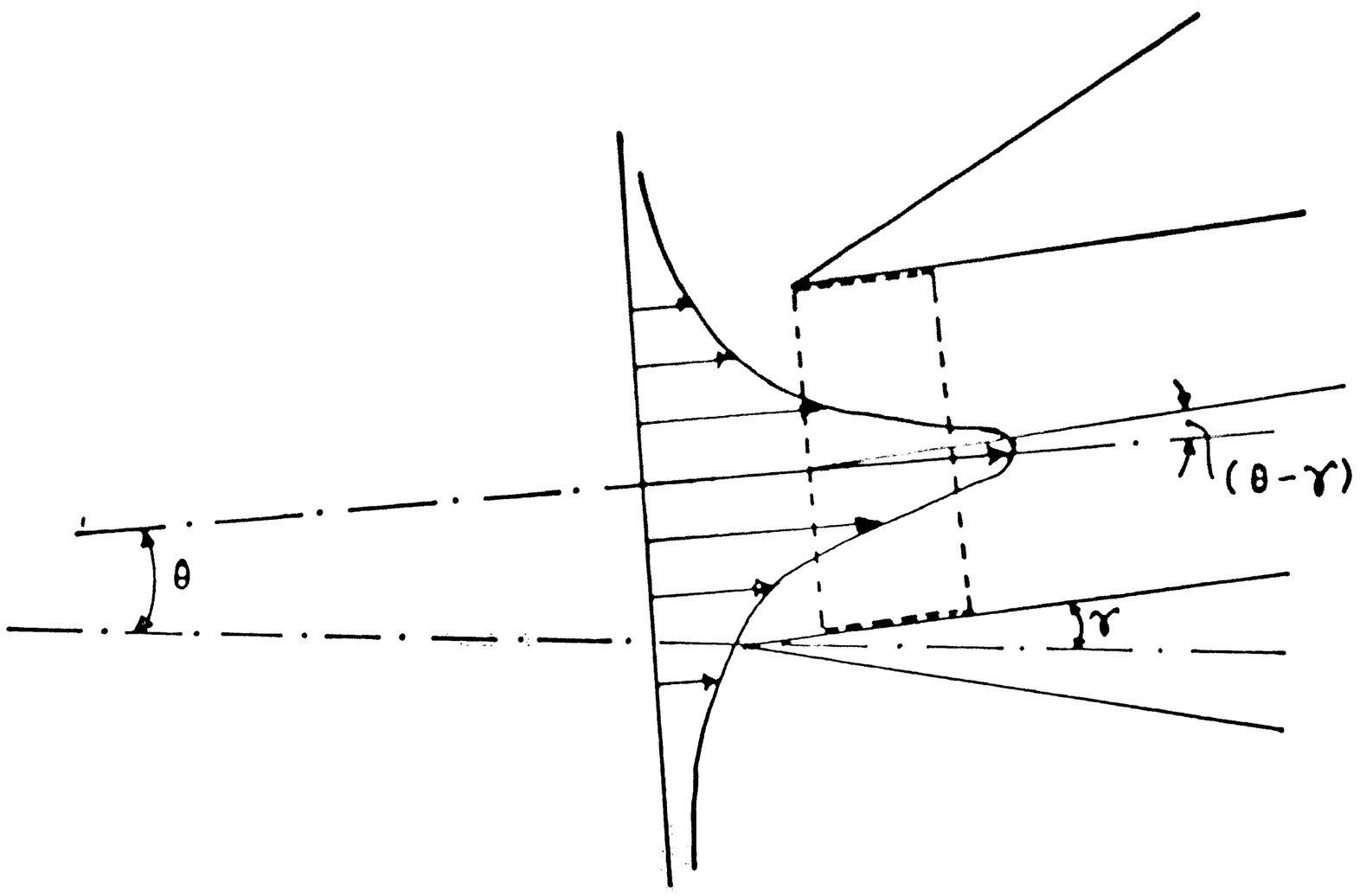

Figure 7. Control Volume for Receiver.

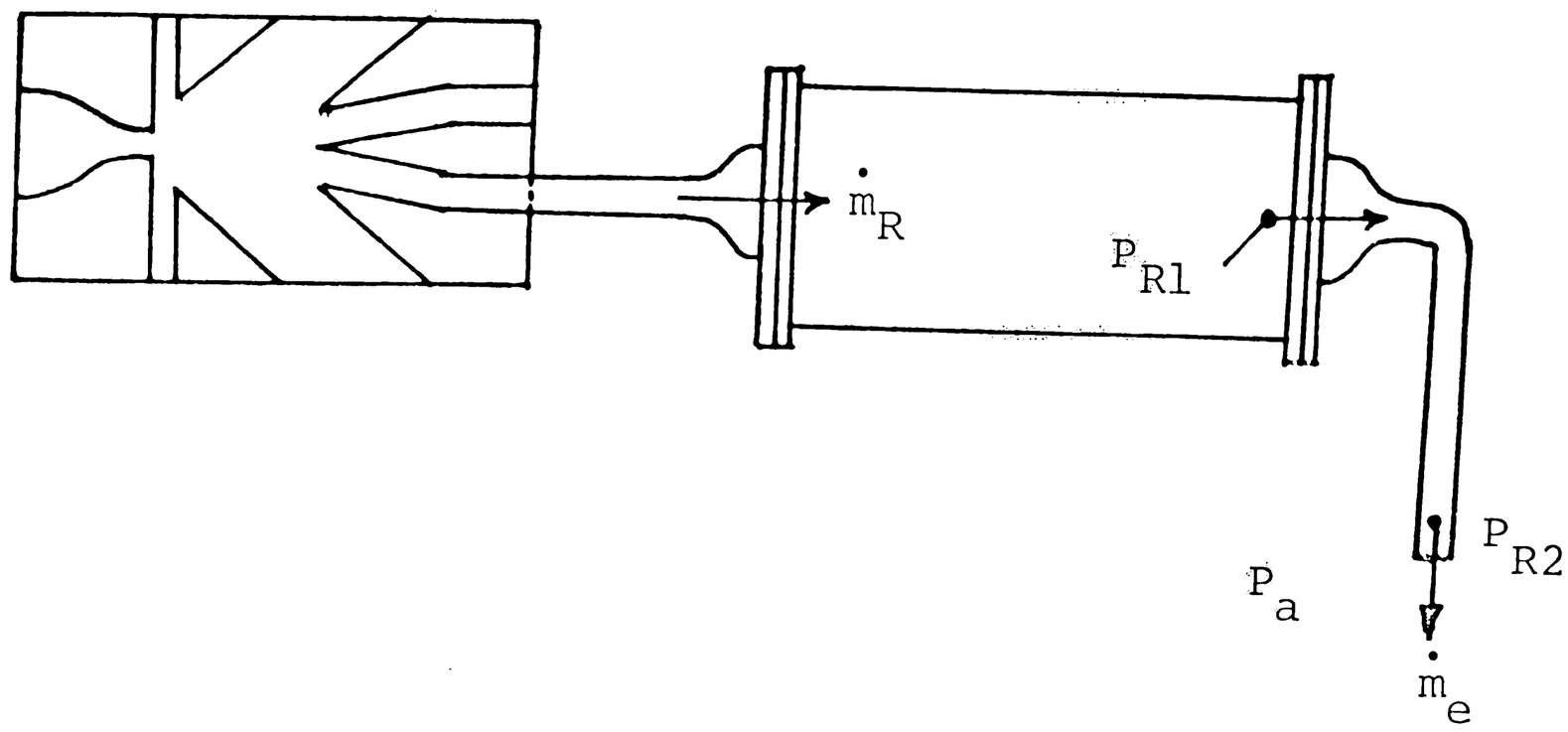

Figure 8. Receiver Line Model.

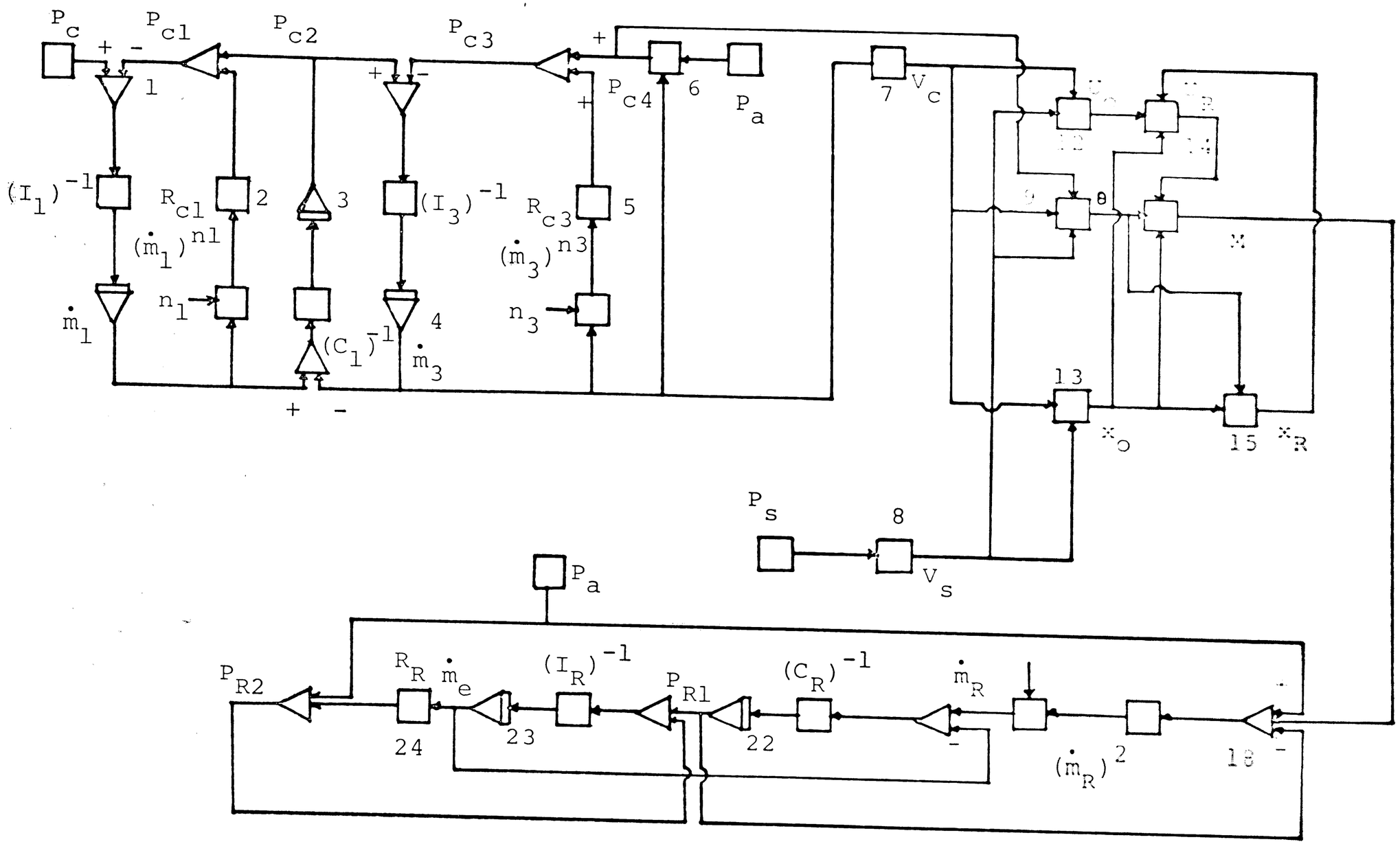

Figure 9. Analog Model for Amplifier Dynamics.

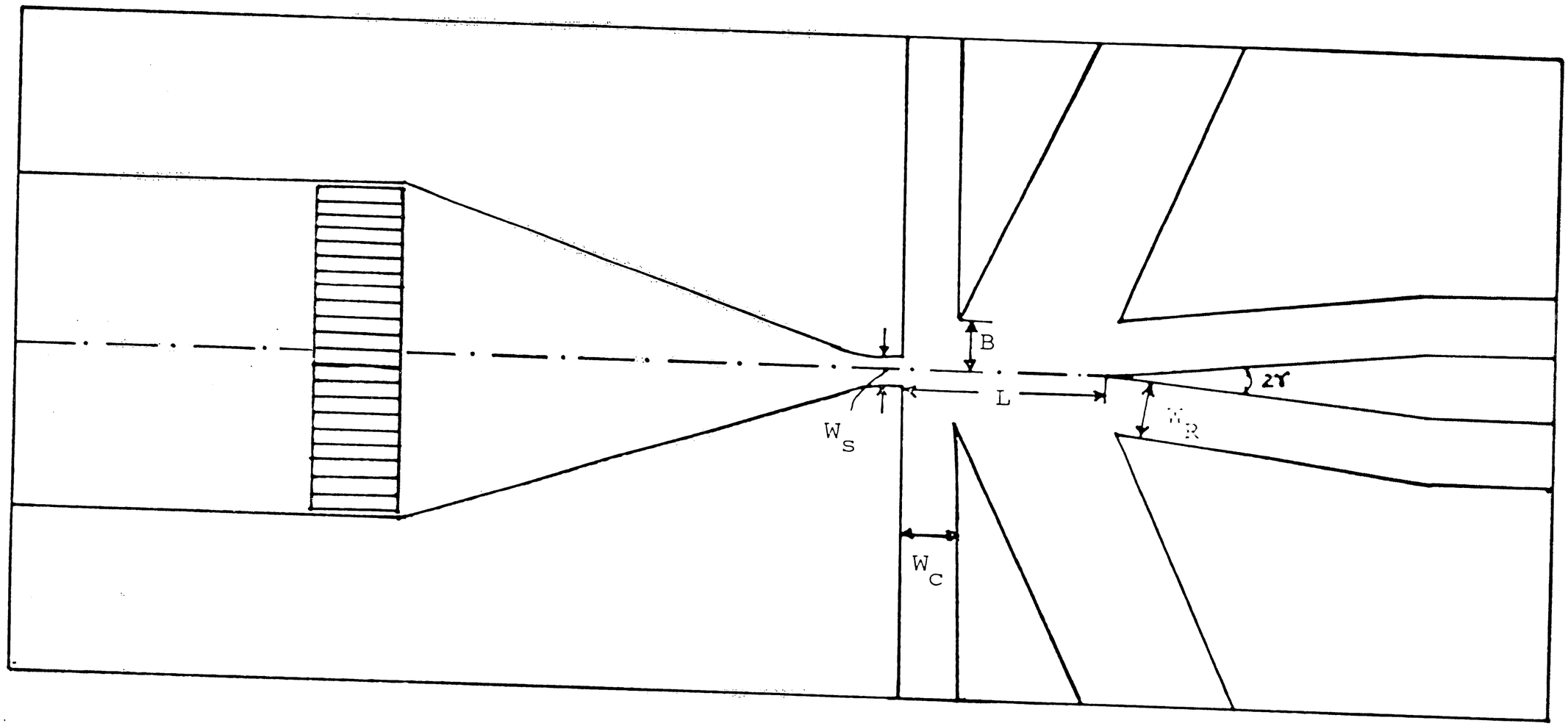

W_C = 0.5 in.
W_R = 0.5 in.
W_S = 0.25 in.

L = 2.5 in.
2γ = 12°

Figure 10. Geometry of Experimental Amplifier.

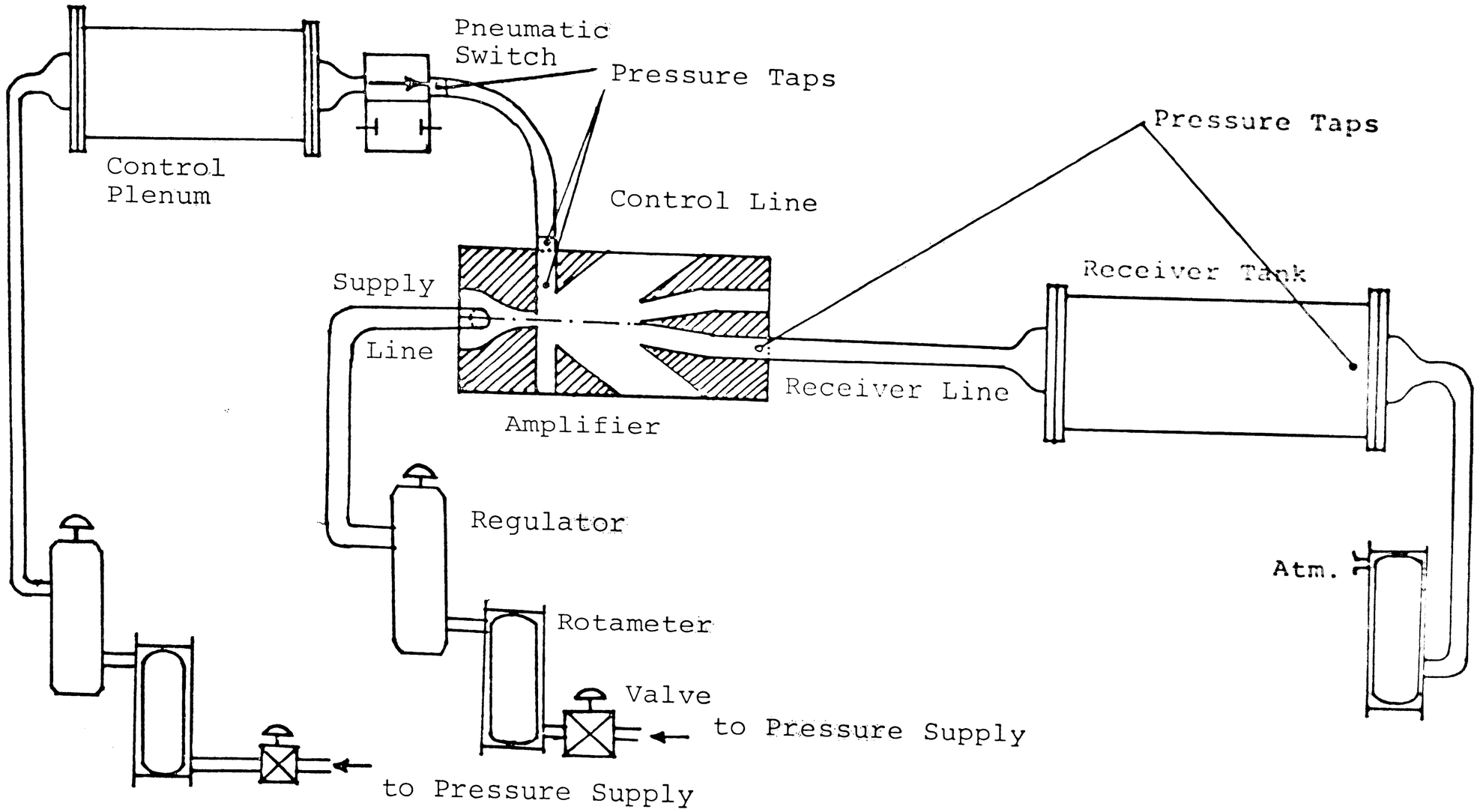

Figure 11. Schematic of Experimental Setup.

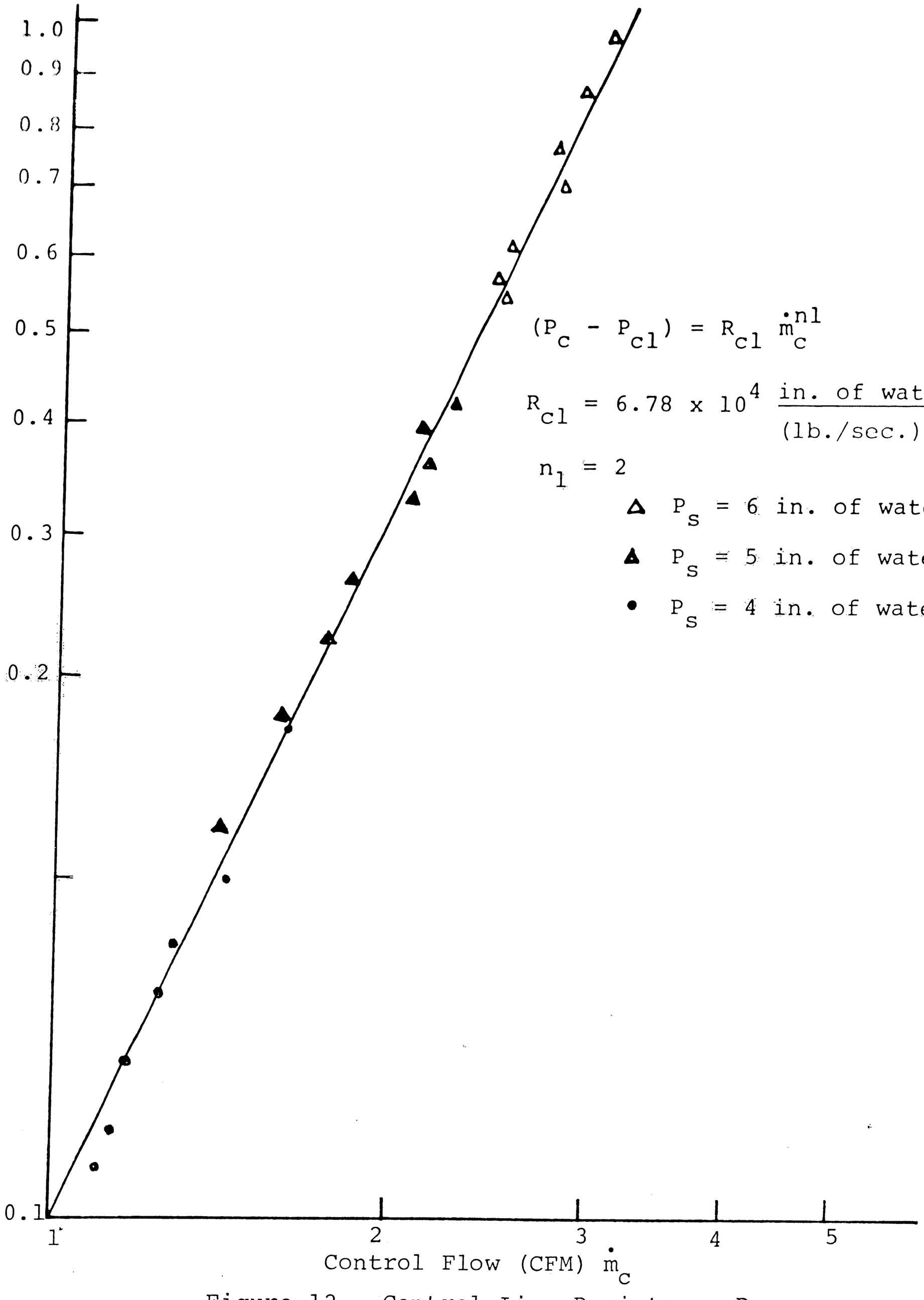

Figure 12. Control Line Resistance R_{cl}

$$P_{c3} - P_{c4} = R_{c3} \dot{m}_c^{n3}$$

$$n_3 = 1.16$$

$$R_{c3} = 1.43 \times 10^2 \ \frac{\text{(in. of water)}}{\text{(lb./sec.)}^{1.16}}$$

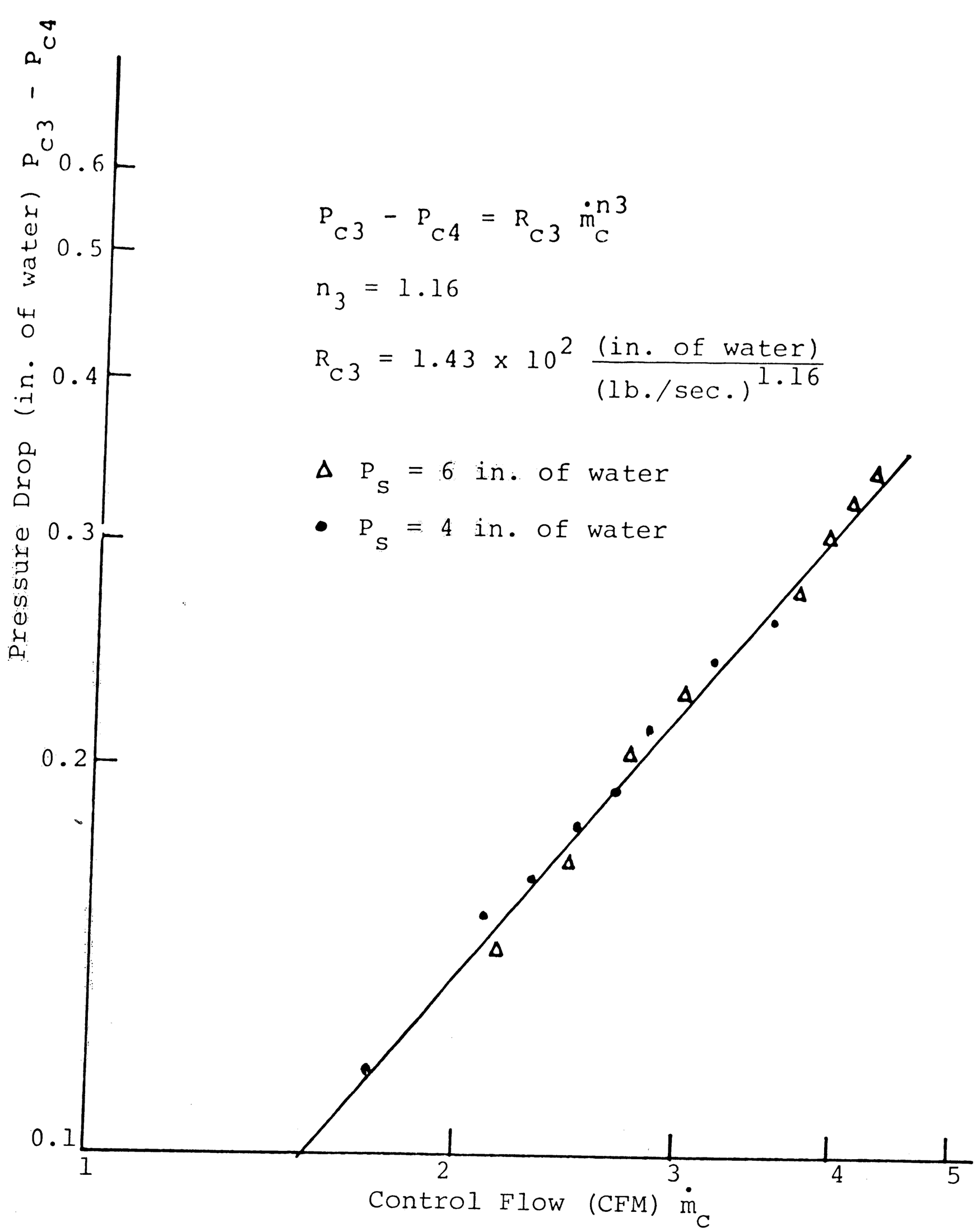

Figure 13. Control Channel Resistance.

$$P_{c4} - P_a = R_{c4}\, \dot{m}_c^{n4}$$

$$n_4 = 1.83$$

$$R_{c4} = 1.11 \times 10^4 \ \frac{\text{(in. of water)}}{(\text{lb./sec.})^{1.83}}$$

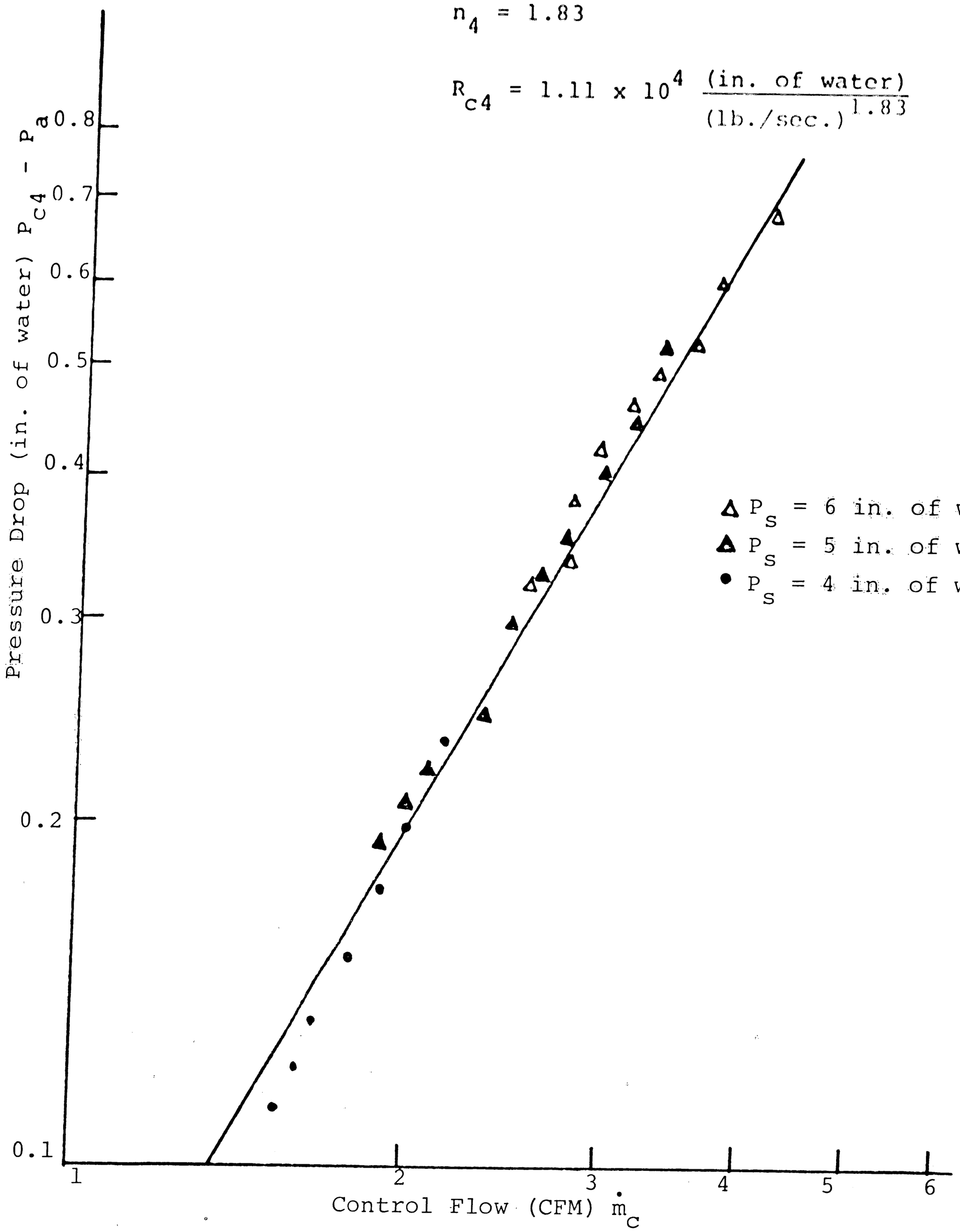

Figure 14. Setback Resistance R_{c4}.

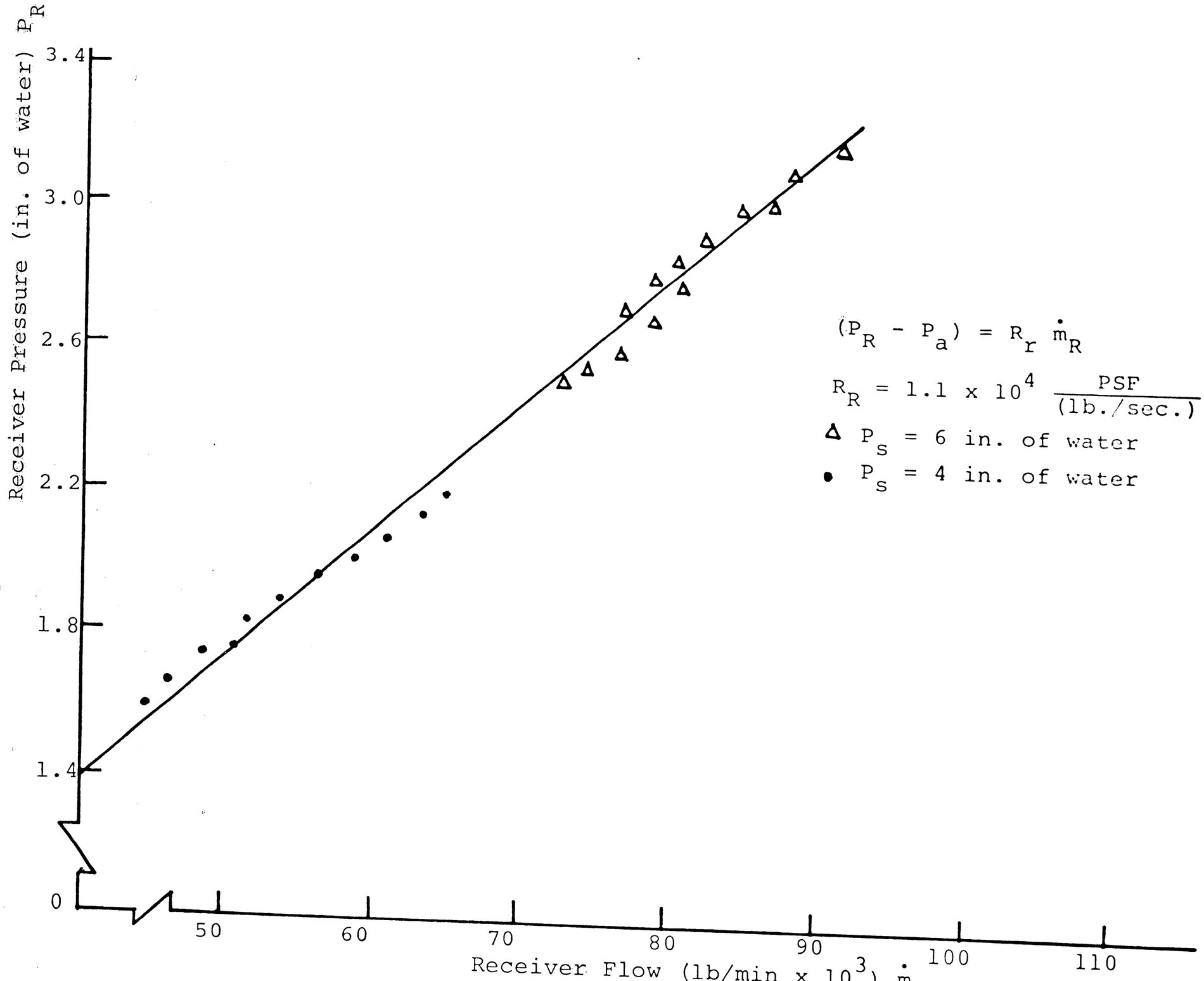

Figure 15. Receiver Line Resistance R_R.

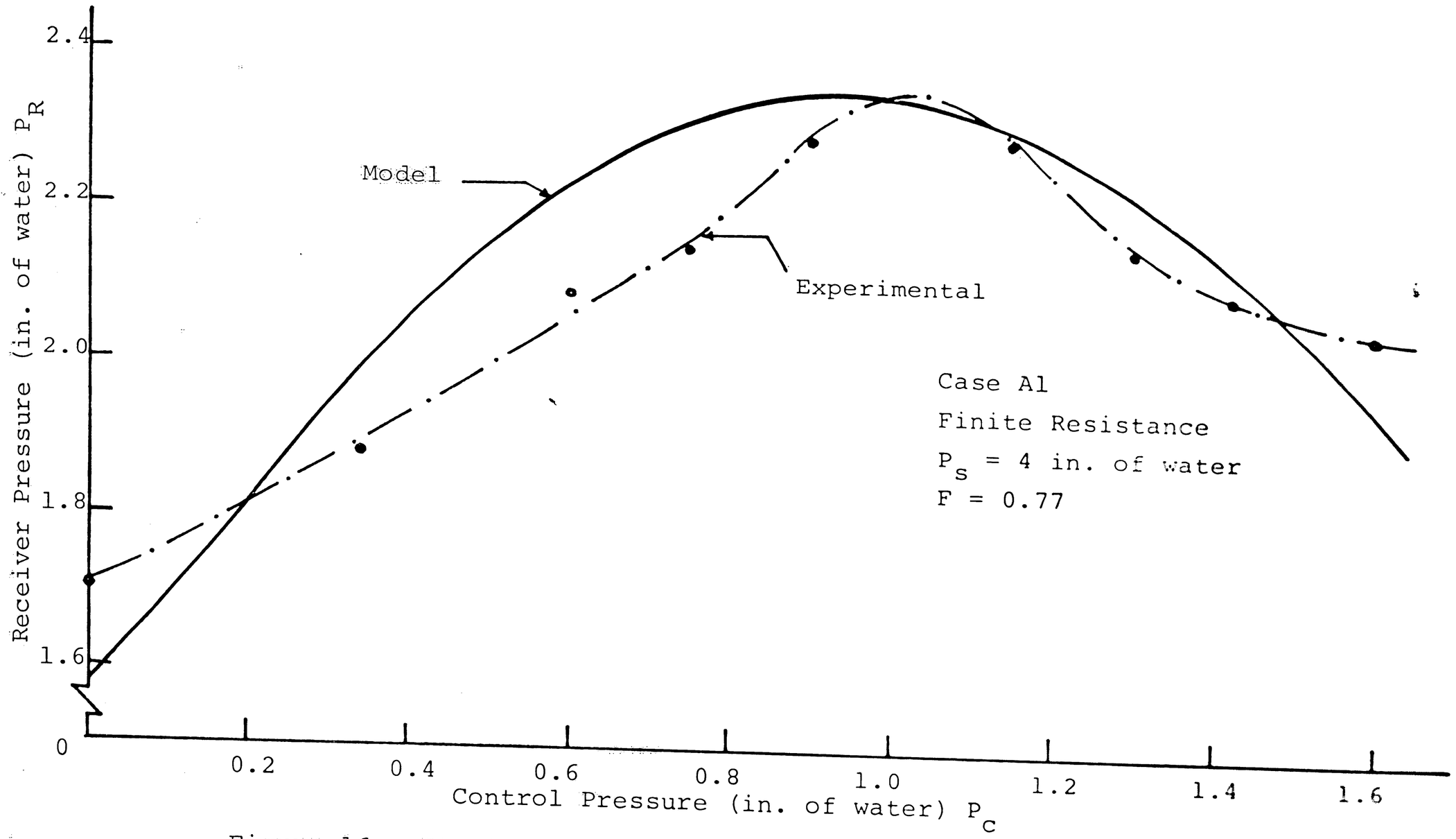

Figure 16. Steady State Pressure Characteristics for Case A1.

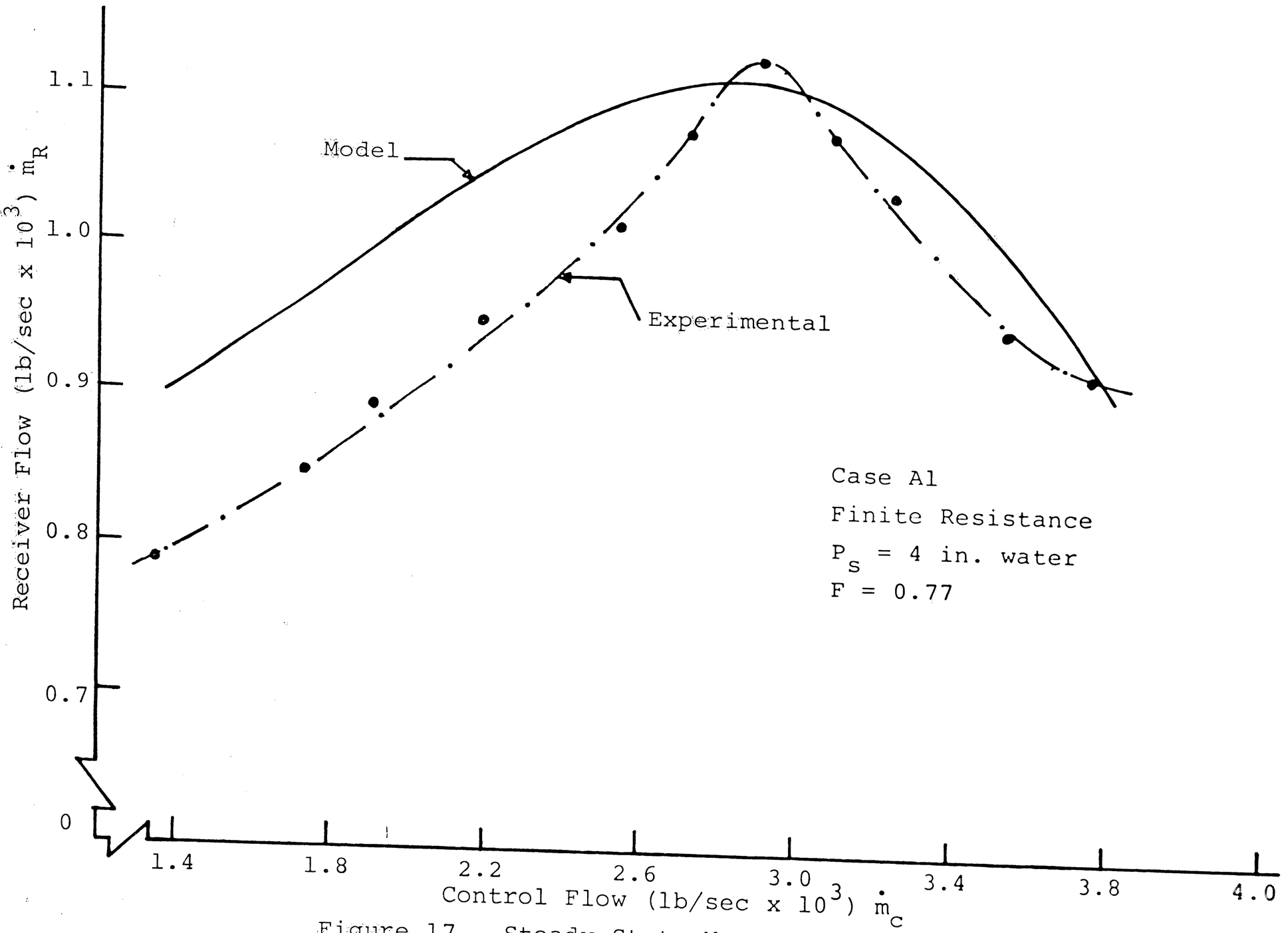

Figure 17. Steady State Mass Flow Characteristics for Case A1.

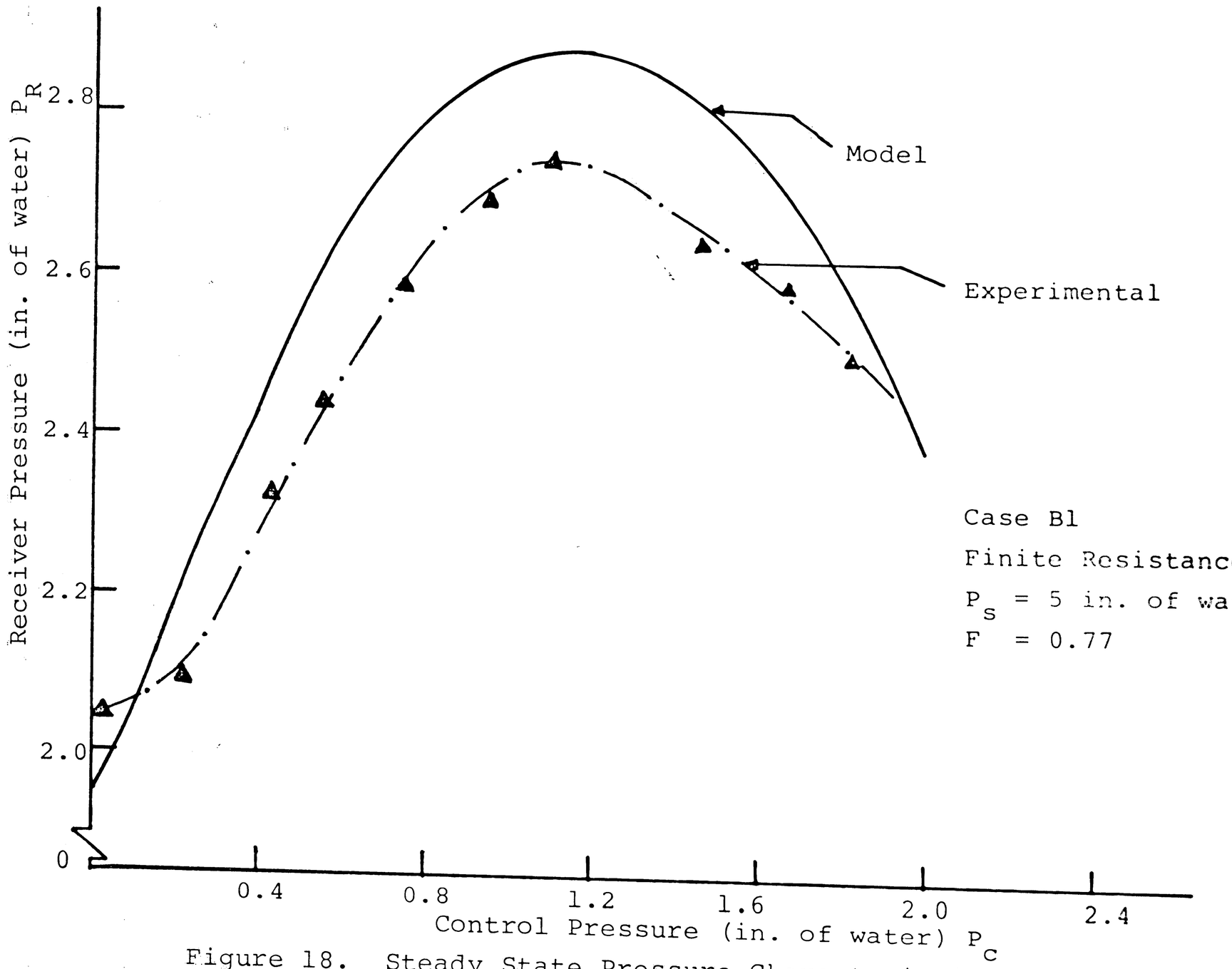

Figure 18. Steady State Pressure Characteristics for Case B1.

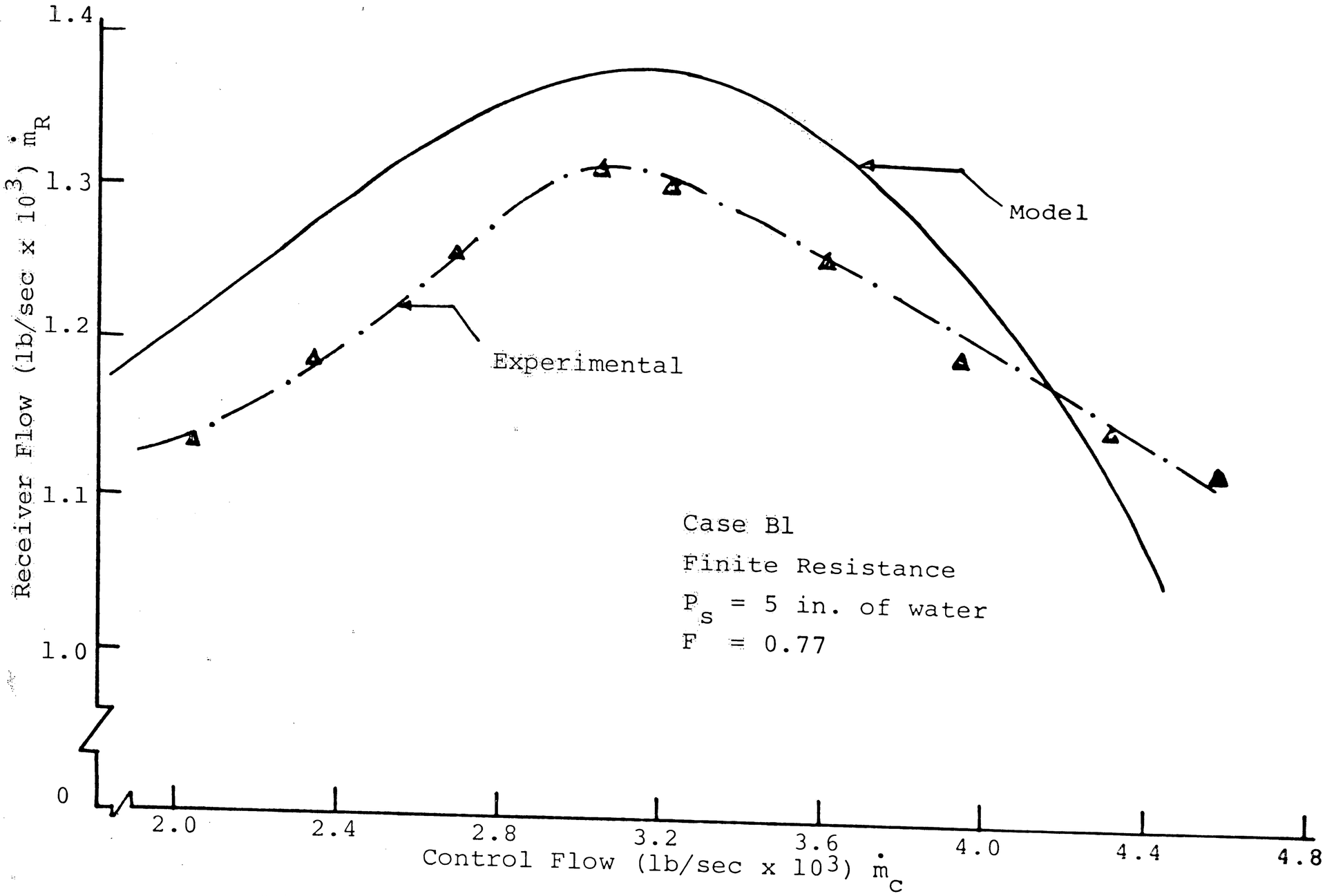

Figure 19. Steady State Mass Flow Characteristics for Case B1.

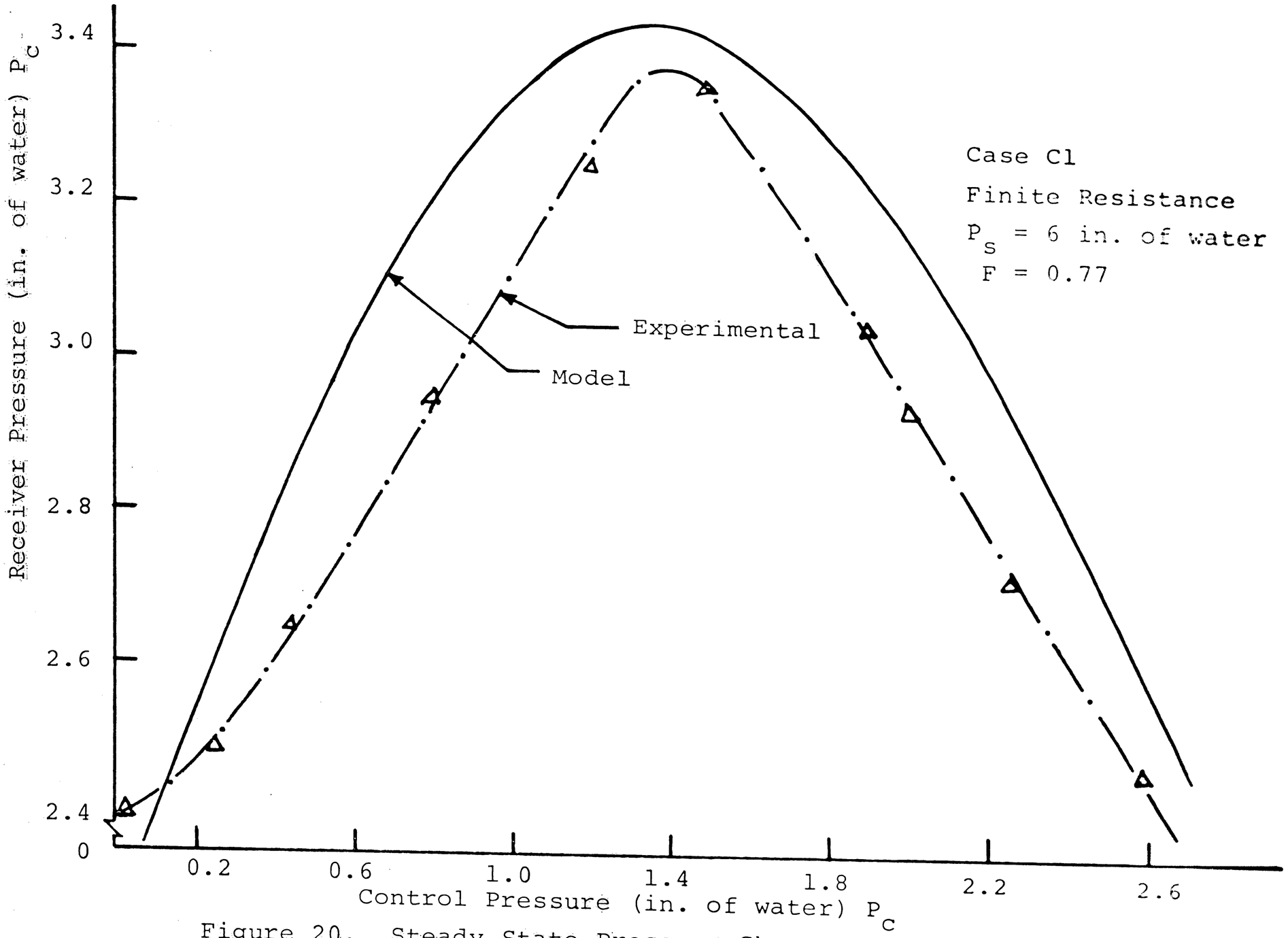

Figure 20. Steady State Pressure Characteristics for Case C1.

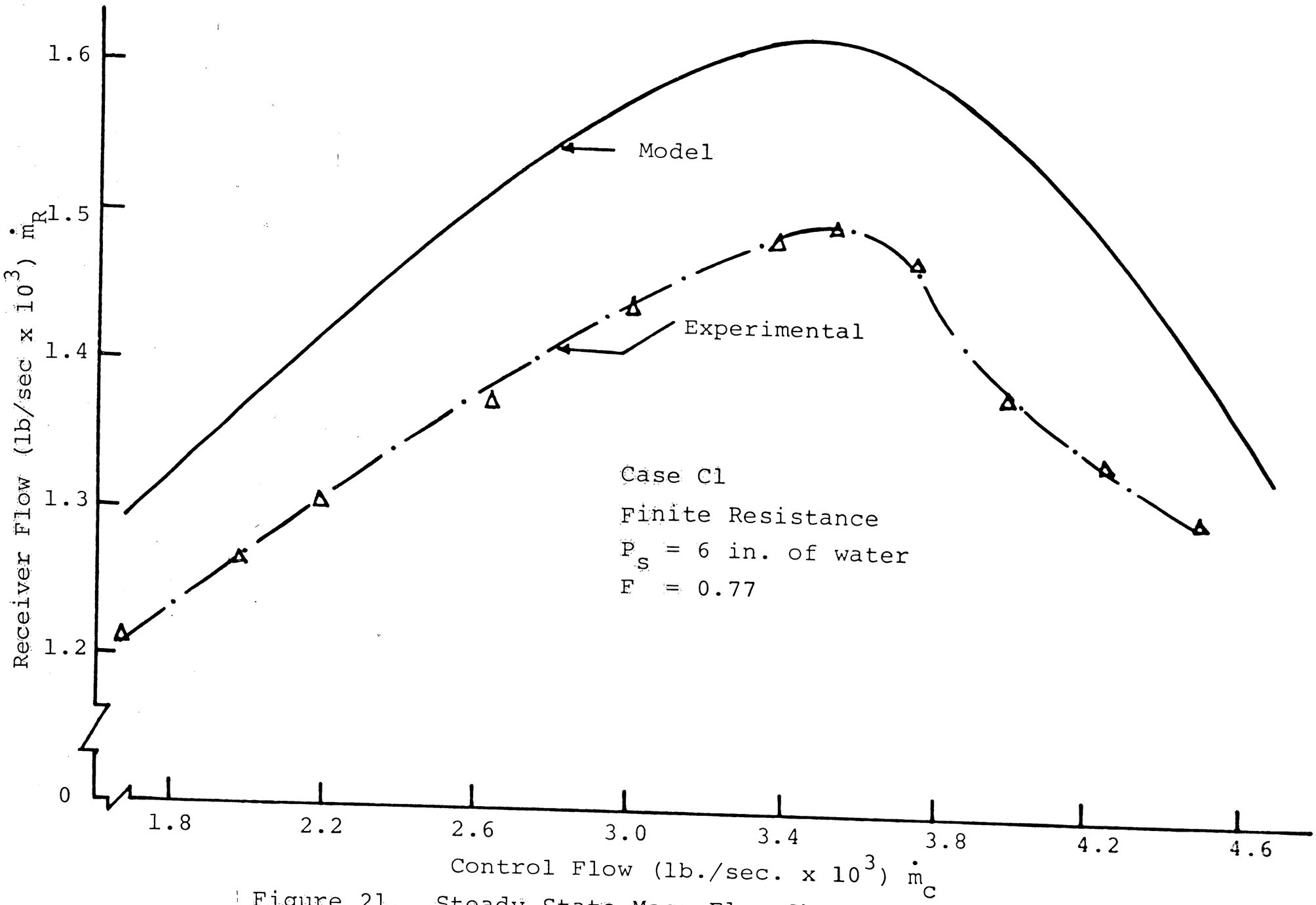

Figure 21. Steady State Mass Flow Characteristics for Case C1.

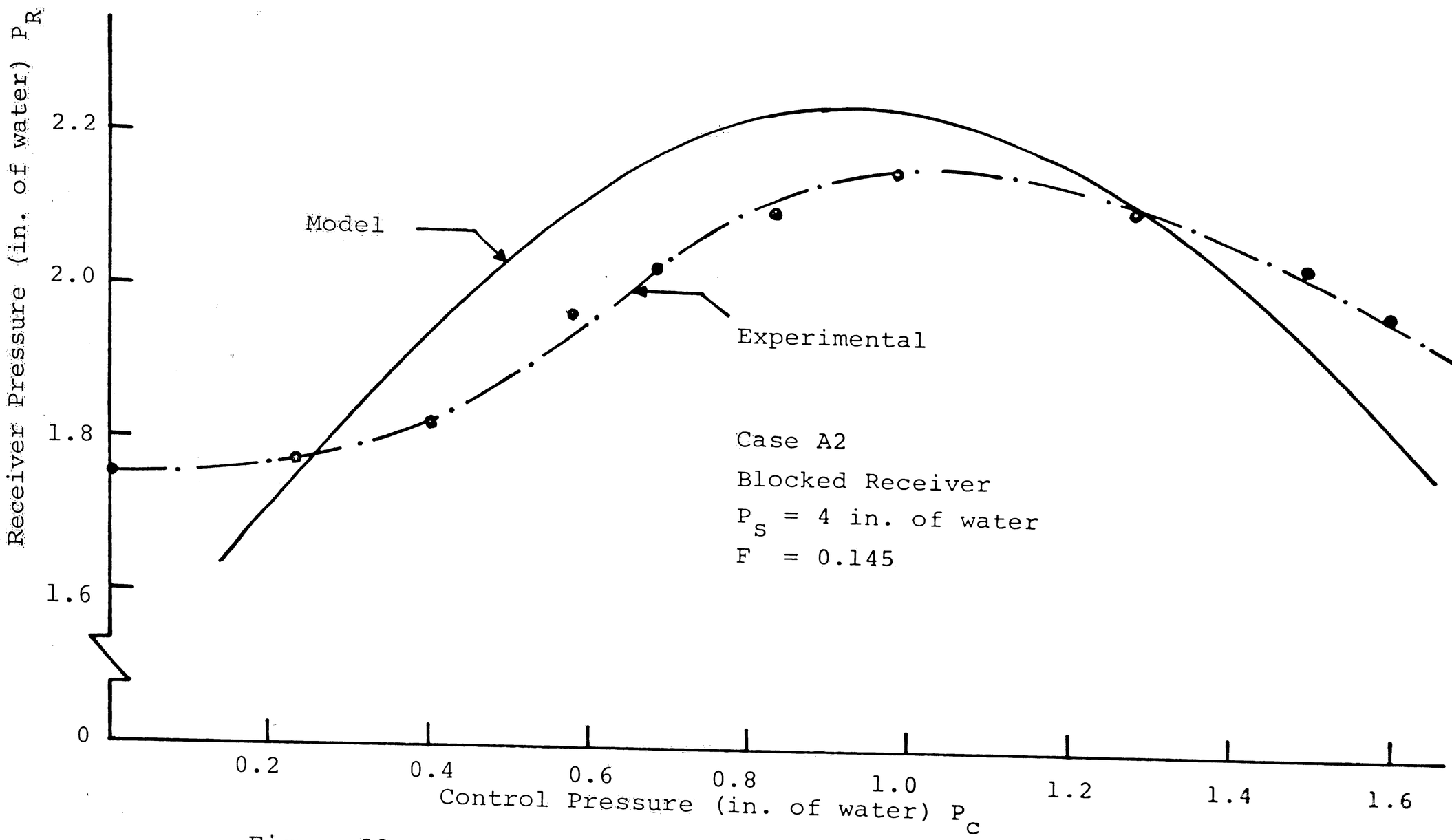

Figure 22. Steady State Pressure Characteristics for Case A2.

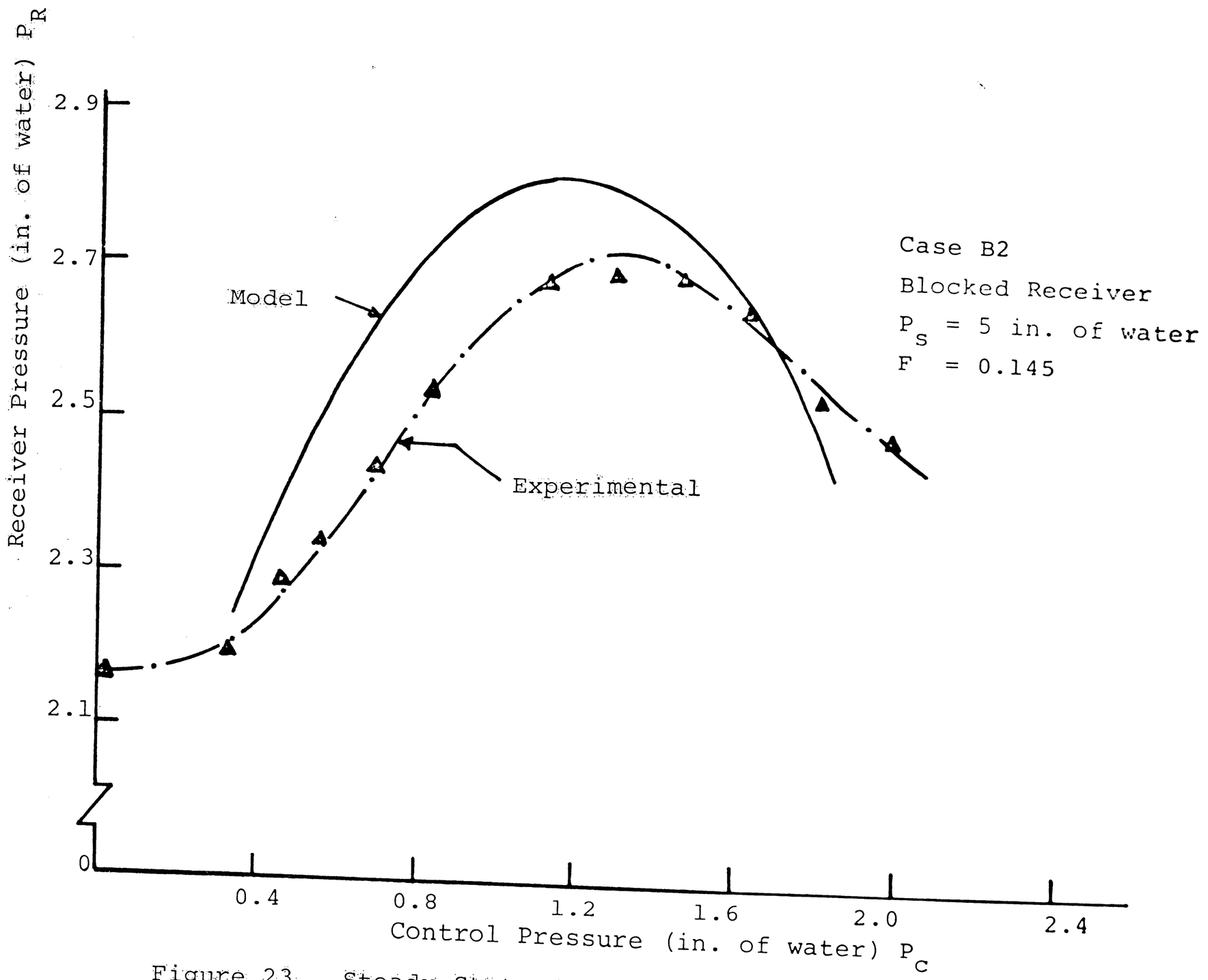

Figure 23. Steady State Pressure Characteristics for Case B2.

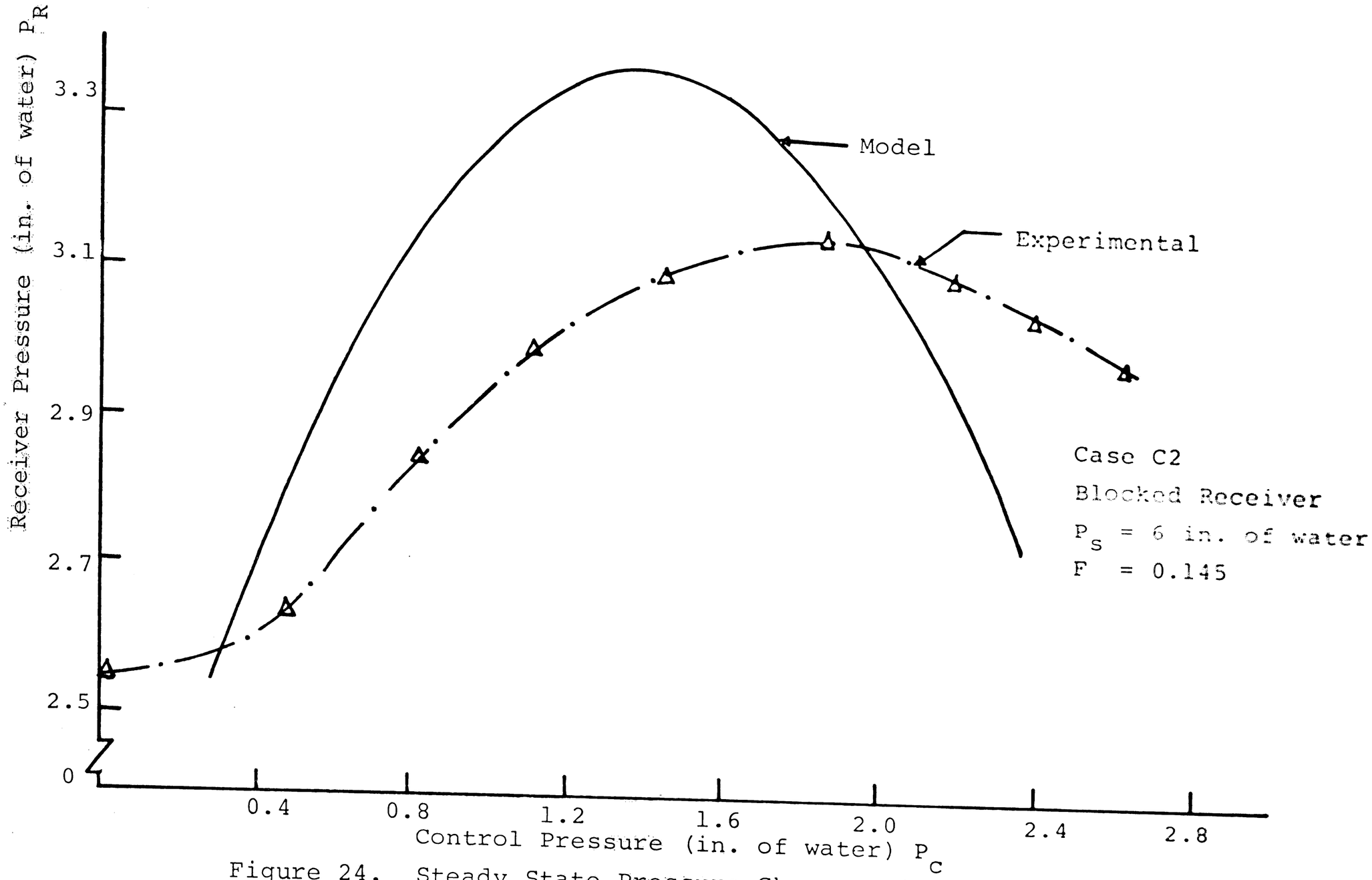

Figure 24. Steady State Pressure Characteristics for Case C2.

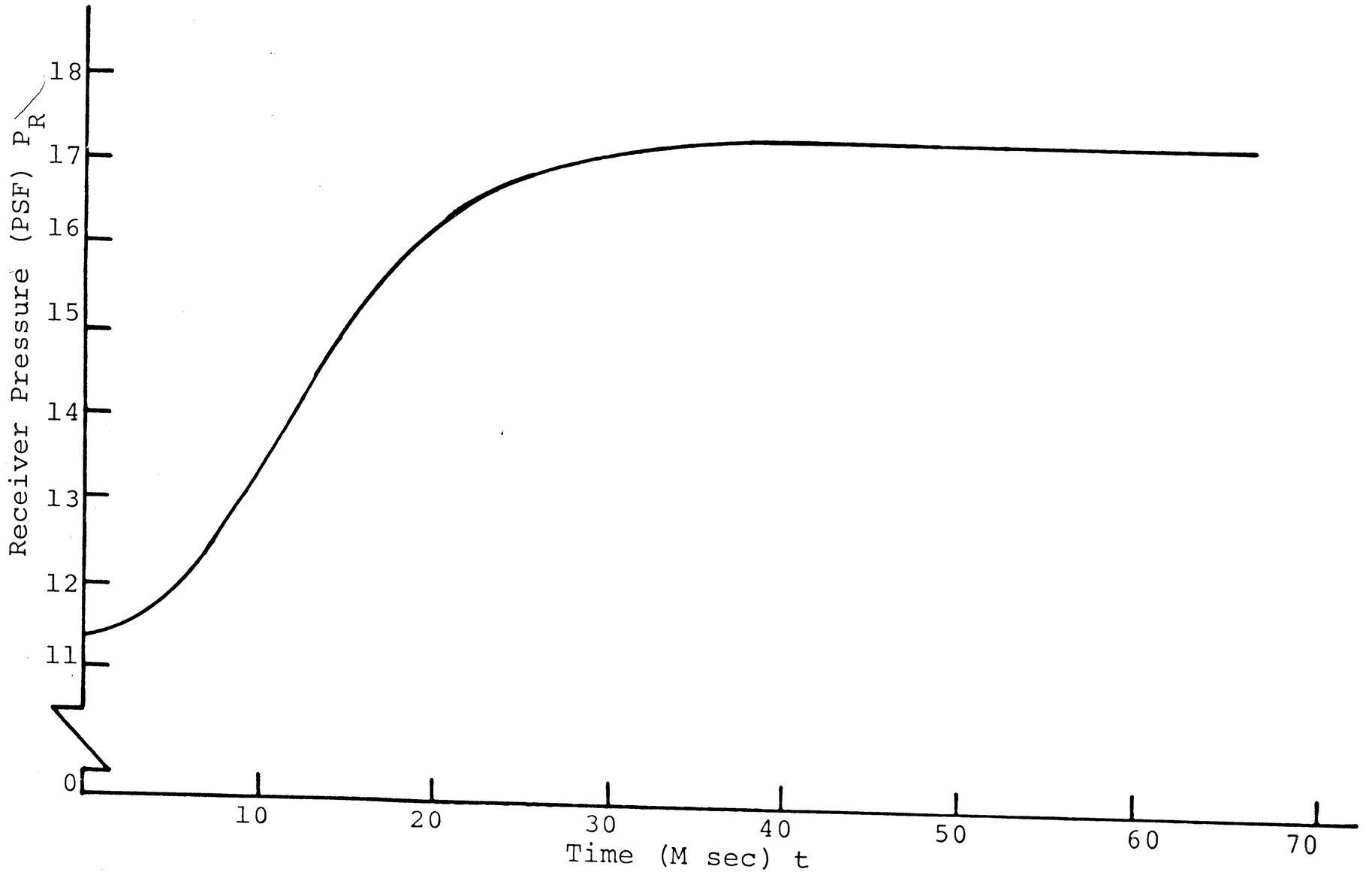

Figure 25. Analytical Dynamic Response (Without Edge-tone Effect).

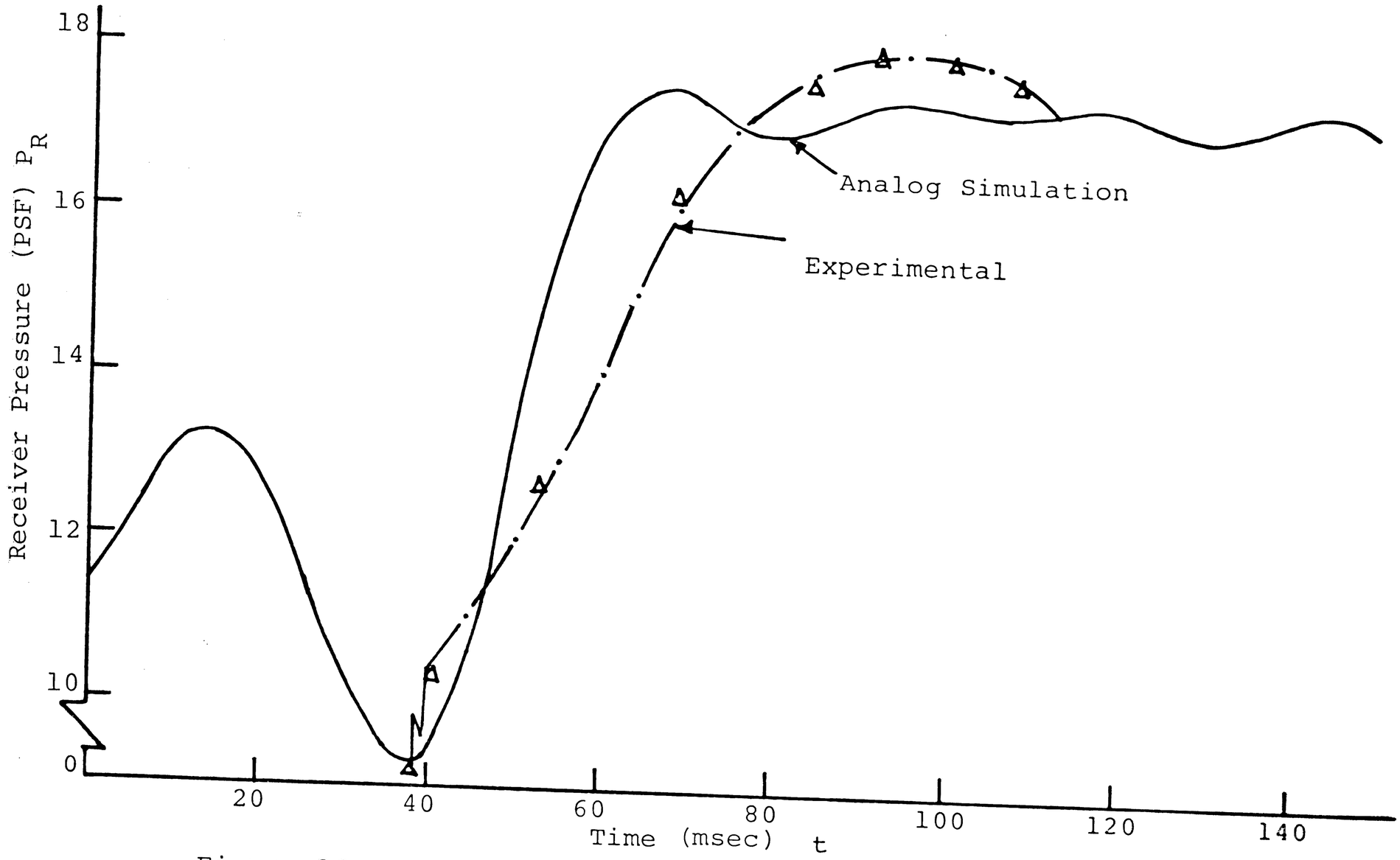

Figure 26. Dynamic Response to Step Input at t = 37.5.

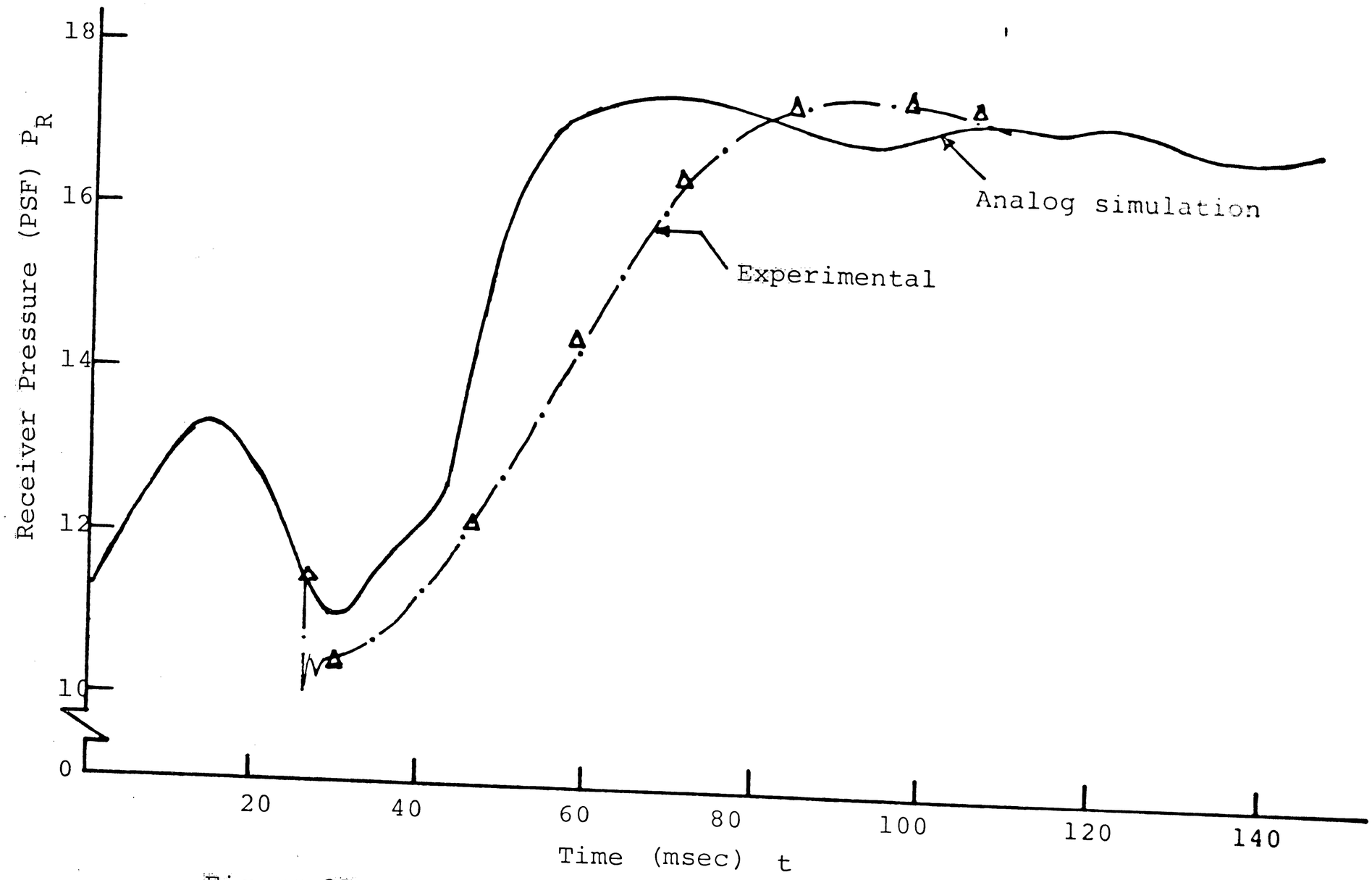

Figure 27. Dynamic Response to Step Input at t = 25.

REFERENCES

1. Abramovich, G. N., The Theory of Turbulent Jets, The MIT Press, Cambridge, Massachusetts, 1963.

2. Albertson, M. L., et al, "Diffusion of Submerged Jets", Proc. Am. Soc. of Civil Engrs., Vol. 74, 1948.

3. Ezekial, F. D. and Paynter, H. M., "Computer Representations of Engineering Systems Involving Fluid Transients", Trans. ASME, Vol. 79, 1957.

4. Heck, K. C., "Design and Analysis of a Jet Interaction Fluid Amplifier", M. S. Thesis, Lehigh University, Bethlehem, Pa., 1972.

5. Kallevig, J. A., "Effect of Receiver Design on Amplifier Performance and Jet Profile of a Proportional Fluid Amplifier", Proc. of the Fluid Amplification Symposium, Harry Diamond Laboratories, Vol. II, October 1965.

6. Kirshner, J. M., Fluid Amplifiers, McGraw-Hill, New York, 1966.

7. Manion, F., "Proportional Amplifier Simulation", Advances in Fluidics, ASME, May 1967.

8. Morris, S. M. and Schiesser, W. E., "Lehigh Analog Simulator (LEANS)", 1965, 1970.

9. Moses, H. L. and McRee, D. I., "Switching in Digital Fluid Amplifiers", ASME Paper No. 69-FLCS-31.

10. Olson, R. E. and Camarata, J. F., "Pressure Recovery Characteristics of Compressible Two-Dimensional Free Jet Flows", Proc. of the Fluid Amplification Symposium, HDL, Vol. I, October 1965.

11. Powell, E. A. and Bidgood, R. E., "An Investigation into the Design of a Beam Deflection Type of Proportional Amplifier", Third Cranfield Fluidics Conference, Vol. 2, 1968.

12. Rupert, J. G., "Analysis of the Pressure Flow Characteristics of a Submerged Jet-Receiver-Diffuser-Load System", National Conference on Fluid Power, 23rd Annual Meeting, October 19-20, 1967.

13. Sarpkaya, T., et al, "A Theoretical and Experimental Investigation of the Interaction of Jets in Beam-Deflection Type Fluidic Elements:", Fourth Cranfield Fluidics Conference, 1970.

14. Schlichting, H., Boundary Layer Theory, McGraw-Hill, New York, 1968.

15. Tollmien, W., "Berechnung Turbulenter Ausbreitungs-Vorgänge", ZAMM, Vol. 6, 1926.

VITA

Shiraz Rehmani, son of Yusuf and Mehrunissa Rehmani, was born on February 4, 1949 at Bombay, India. He obtained his Secondary School Certificate in August, 1962 and his Higher Secondary Certificate in August, 1964 from the Board of Secondary Education, Karachi. He did his undergraduate studies at the N. E. D. Government Engineering College, Karachi. He received his B. M. E. degree in November, 1970 and was awarded a Gold Medal by the University of Karachi for graduating at the head of his class.